HIGH-TEMPERATURE ETHANE DEHYDROGENATION IN MICROPOROUS ZEOLITE MEMBRANE REACTOR: EFFECT OF OPERATING CONDITIONS

By

SHAILESH SINGH DANGWAL

Bachelor of Technology-Chemical Engineering

Indian Institute of Technology Guwahati

Guwahati, India

2012

Submitted to the Faculty of the
Graduate College of the
Oklahoma State University
in partial fulfillment of
the requirements for
the Degree of
MASTER OF SCIENCE

July, 2017

HIGH-TEMPERATURE ETHANE DEHYDROGENATION IN MICROPOROUS ZEOLITE MEMBRANE REACTOR: EFFECT OF OPERATING CONDITIONS

Thesis Approved:

Dr. Seok Jhin Kim

Thesis Adviser

Dr. Sundar Madihally

Dr. Heather Fahlenkemp

ACKNOWLEDGEMENTS

Firstly, I would like to thank my advisor Dr. Seok-Jhin Kim for his enormous help and continuous guidance during the last one and a half year. He has been a great mentor who has always inspired and kept me motivated which eventually helped me in finishing my tasks. Under his able guidance, I was involved in the establishment of our lab and learned a lot about membranes. The most important thing which I learned from him is hard work, honesty towards work and organization skills. Moreover, I would also like to thank my committee members Dr. Sundar Madihally and Dr. Heather Fahlenkemp for agreeing to serve on my thesis committee.

I am grateful to the School of Chemical Engineering at OSU for their financial support throughout this program. I am also thankful to all the professors, faculty and staff at OSU for their continuous help and support.

I would also like to thank my lab mate Ruochen Liu for his for his help and support. He was always ready to offer his insights and suggestions. I am also grateful to my colleague Sushobhan Pradhan who helped me a lot in learning the software Origin, which helped me in refining plots, depicted in this work.

I would also like to thank to all my friends and colleagues at OSU. Without their love and support this work would not have been possible. I am grateful to Mukesh Singh, Rajesh Tolety and Barkha Dua for always being there for me throughout this journey.

Lastly I would like to thank my parents, Mrs Jeeta Dangwal and Mr Virendar Dangwal. I would not have been able to achieve all this, had it not been for their support. I am forever indebted to them and they are the reason for all my accomplishment.

Name: Shailesh Singh Dangwal

Date of Degree: June, 2017

Title of Study: HIGH-TEMPERATURE ETHANE DEHYDROGENATION IN MICROPOROUS ZEOLITE MEMBRANE REACTOR: EFFECT OF OPERATING CONDITIONS

Major Field: CHEMICAL ENGINEERING

Abstract: Ethylene is the largest base chemical for the chemical industry and produced either by cracking or dehydrogenation of light alkanes. The increasing demand for ethylene has stimulated substantial research into the development of new processes to reduce energy consumption. The ethane dehydrogenation reaction (EDH) using a membrane reactor is an attractive solution because the equilibrium limit can be overcome in favor of ethylene by selective removal of H_2. The process intensification of EDH reaction was studied in packed-bed membrane reactors (PBMR) operating with a Pt/Al_2O_3 catalyst. The effects of MFI-type zeolite PBMR and operating conditions on ethane conversion, ethylene selectivity, and ethylene yield were investigated. MFI membrane reactors allowed the equilibrium limit of ethane conversion to be surpassed at high temperatures. It was demonstrated that medium-pore MFI membranes with moderate H_2/C_2H_6 selectivity can effectively improve ethane conversion at high operation temperature by timely removal of H_2 through the membranes. The experiment results showed that using MFI zeolite membrane with separation factor of 3.3 for H_2/C_2H_6 and H_2 permeance of 1.2×10^{-7} mol m^{-2} s^{-1} Pa^{-1} at 600 °C helped in enhancing the ethane conversion, ethylene selectivity and ethylene yield from 12%, 86 %, and 10% for the packed bed reactor (PBR) to 24%, 90% and 22% for the PBMR respectively. The model calculations have shown that near-completion ethane conversion > 98% may be achieved under practically meaningful operating temperature, pressure, and space velocity even for membranes with moderate H_2 selectivity and permeance.

TABLE OF CONTENTS

LIST OF TABLES vii
LIST OF FIGURES viii
CHAPTER I INTRODUCTION 1
1.1 Global Ethylene Production 1
1.2 Sources of Ethylene 2
1.3 Method of Ethylene Production 3
1.4 Thesis Objective 4

CHAPTER II BACKGROUND AND LITERATURE REVIEW 6
2.1 Zeolites and Zeolite Membrane 6
2.2 Zeolite membrane reactors 8
2.3 Review of EDH 8

CHAPTER III SYNTHESIS OF MFI TYPE ZEOLITE MEMBRANE 11
3.1 Preparation of Membrane 11
3.2. Membrane Properties 12
3.2.1 Membrane Performance Parameters 12
3.2.2 Zeolite Membrane Properties 13
3.3 Summary 17

CHAPTER IV HIGH TEMPERATURE EDH REACTION IN MICROPOROUS ZEOLITE MEMBRANE REACTOR 18
4.1 Experimental 18
4.1.1 EDH Reaction 18
4.2 Results and Discussions 21

4.2.1 Effect of Reaction Temperature…….21
4.2.2 Effect of Space Velocity…….24
4.2.3 Effect of Sweep Gas……....25
4.2.4 Methanation…….27
4.2.5 Effect of H_2 Addition……..28
4.3 Summary……...31

Chapter V MODELLING AND SIMULATION OF HIGH TEMPERATURE EDH REACTION IN MFI ZEOLITE MEMBRANE REACTOR……...33
5.1 Model for EDH MR Simulation……..……..33
5.1.1. Kinetic Equations……..33
5.1.2. Membrane Gas Permeance……36

5.2 EDH MR Simulation…….37
5.2.1 Model Validation……....37
5.2.2 Model Calculation……..38

5.3 Summary…….....47

Chapter VI CONCLUSIONS 49
BIBILOGRAPHY OF SHALESH SINGH DANGWAL……..51
REFERENCES……...52
APPENDIX 58

LIST OF TABLES

Table 1: H_2/CO_2 separation factor variation at room temperature for different zeolite membranes…….....14

Table 2: Separation properties for H_2/C_2H_4 equimolar mixture before and after EDH reaction …….16

Table 3: EDH membrane reactor conditions……...21

Table 4: Parameters for evaluating membrane permeation properties…….....36

LIST OF FIGURES

Figure 1: Global Ethylene consumption year wise…….....1
Figure 2: Ethylene capacity growth region wise over the years……..2
Figure 3: Ethylene production over the years by Feedstock……...3
Figure 4: Steam Cracking Process……...4
Figure 5: Schematic description of zeolite membrane formation on a porous substrate(a) nucleation on surface and (b) crystal growth in to continuous polycrystalline membrane……..7
Figure 6: SEM images of the secondary grown zeolite MFI membranes: (a) surface and (b) cross section… ……...……13
Figure 7: Performance characteristics of (a) H_2/C_2H_6 and (b) H_2/C_2H_4 equimolar mixtures in MFI zeolite membranes as a function of temperature……15
Figure 8: Permeation characteristics of H_2/C_2H_4 (a) before EDH experiment and (b) after EDH experiment for equimolar mixtures in MFI zeolite membranes as a function of temperature……16
Figure 9: Schematic diagram showing membrane reactor system used for EDH reaction……20
Figure 10: Effect of reaction temperature on (a) ethane conversion, and (b) ethylene selectivity and ethylene yield, in PBMR and PBR (WHSV = 0.45 h^{-1}; F_{Ar} = 20 cm^3/min; and p_{perm} = 1 atm)……... 22

Figure 11: Effect of temperature on molar concentration of ethane, ethylene and H_2 for (a) PBMR retentate, (b) PBMR permeate and (c) PBR. (*WHSV* = 0.45 h^{-1}; F_{Ar} = 20 cm^3/min; and p_{perm} = 1 atm)……... 23
Figure 12: Effect of WHSV on (a) ethane conversion, and (b) ethylene selectivity and ethylene yield, in the PBMR and PBR (temperature = 600 °C; F_{Ar} = 20 cm^3/min; and p_{perm} = 1 atm)….. 24
Figure 13: Effect of F_{Ar} on (a) ethane conversion, and (b) ethylene selectivity and ethylene yield, in PBMR and PBR (temperature = 600 °C; WHSV = 0.45 h^{-1}; and p_{perm} = 1 atm)…….. 25
Figure 14: Effect of F_{Ar} on molar concentration of ethane, ethylene and H_2 for (a) PBMR retentate, (b) PBMR permeate and (c) PBR (temperature = 600 °C; *WHSV* = 0.45 h^{-1}; and p_{perm} = 1 atm).. 26
Figure 15: Effect of (a) WHSV on methane selectivity and (b) temperature on methane selectivity for PBR and PBMR for (temperature = 600 °C; WHSV = 0.45 h^{-1}; and F_{Ar} = 20 cm^3/min)…… 28
Figure 16: Effect of H_2 concentration in feed on (a) ethane conversion (b) ethylene selectivity (c) ethylene yield, and (d) conversion of ethane with time for Temperature of 600 °C and WHSV of 0.45 h^{-1} for feed (50% ethane and 50% H_2)-10 cm^3/min……30
Figure 17: Schematic showing the gas flow arrangement and mass balance in the PBMR …….35

Figure 18: Experimental and simulated ethane conversion for PBMR and PBR as a function of (a) temperature for WHSV = 0.45 h^{-1} and F_{Ar} = 20 cm^3/min and (b) WHSV for 600 °C and F_{Ar} = 20 cm^3/min, and (c) F_{Ar} for temperature = 600 °C and WHSV =0.45 h^{-1}, respectively……38
Figure 19: Calculated ethane conversion as a function of (a) the reaction temperature and pressure (WHSV = 0.45 h^{-1} and F_{Ar} = 20 cm^3/min) and (b) the reaction temperature and WHSV (p_{feed} = 1 atm and WHSV = 0.45 h^{-1}), respectively……39
Figure 20: Calculated ethane conversion as a function of (a) temperature and F_{Ar} (p_{feed} = 1 atm and *WHSV* = 0.45 h^{-1}); (b) p_{feed} and F_{Ar} (temperature = 600 °C and *WHSV* = 0.45 h^{-1}); (c) *WHSV* and F_{Ar} (temperature = 600 °C and p_{feed} = 1 atm); and (d) *WHSV* and p_{feed} (temperature = 600 °C and F_{Ar} = 20 cm^3/min) in the PBMR……...40
Figure 21: Effect of H_2 permeance (mol m^{-2} s^{-1} Pa^{-1}) and F_{Ar} (cm^3/min) on ethane conversion for WHSV = 0.45 h^{-1} at (a) 500 °C and (b) 650 °C……42
Figure 22: Effect of normalized membrane area (A/A_0) and temperature on ethane conversion for (a) pressure of 1 atm and (b) 1.5 atm (WHSV = 0.45 h^{-1} ; and F_{Ar} = 20 cm^3/min)……43
Figure 23: Effect of pressure (atm) and normalized area (A/A0) on ethane conversion for WHSV=0.45 h^{-1} for (a) temperature = 500 °C (b) temperature = 500 °C (c) temperature = 600 °C (d) temperature = 650 °C for feed- ethane 3cm^3/min (100%)……...45
Figure 24 : Calculated ethane conversion as a function of pressure along the reactor length in (a) PBR and (b) PBMR at WHSV = 0.45 h^{-1} and temperature= 600 °C and as a function of temperature along the reactor length (c) PBR and (d) PBMR at WHSV = 0.45 h^{-1} and *pfeed*= 1 atm……47

CHAPTER I

Introduction

1.1 Global Ethylene Production

Ethylene is an important intermediate in petrochemical industry which is used in the production of plastic bags, paints, antifreeze, toys, pipes, windows frames and car components [1]. As it can be seen in Figure 1 majority of the ethylene produced globally is used for the production of polyethylene which is mostly used in the production of polyethylene [2]. Other important ethylene derivatives are ethylene oxide, ethylene dichloride and ethyl benzene [3-5].

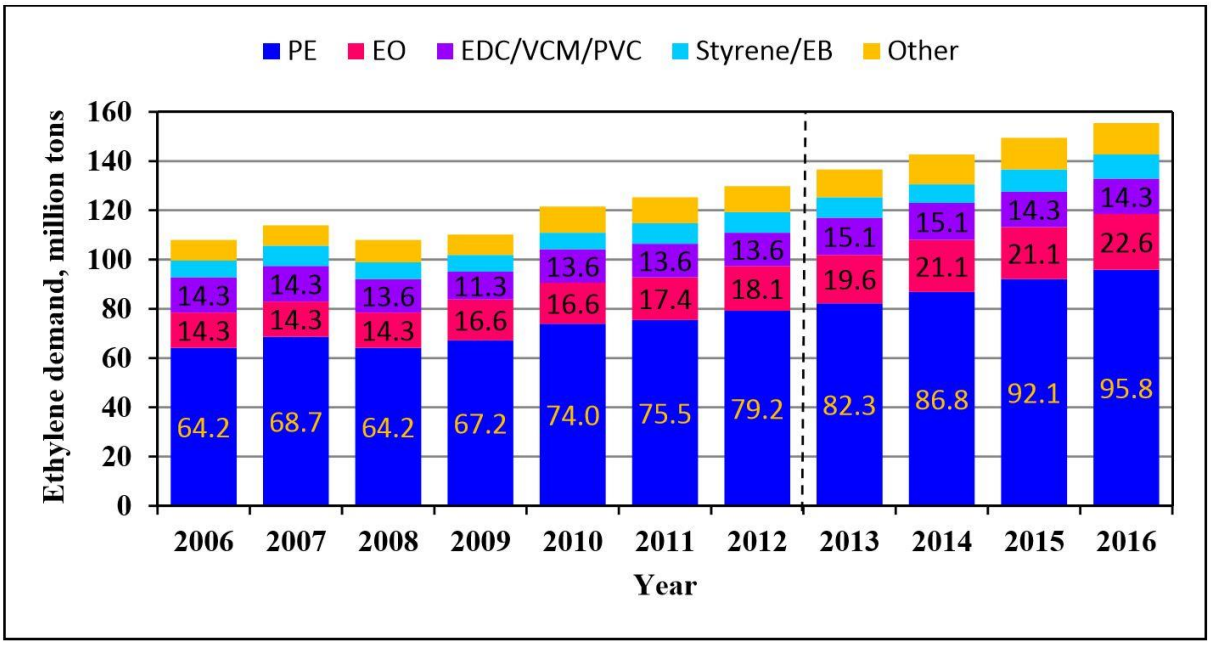

Figure 1. Global Ethylene consumption year wise [2].

Global ethylene capacity has been steadily increasing since 1995 which can be seen in Figure 2 . Asia pacific and middle east were two fastest increasing regions. In 2013 the global ethylene production was 143 million tons versus 141 million tons in 2012 [6]. The largest ethylene plant is in Mailiao, Taiwan with the capacity of 2.94 million tons.

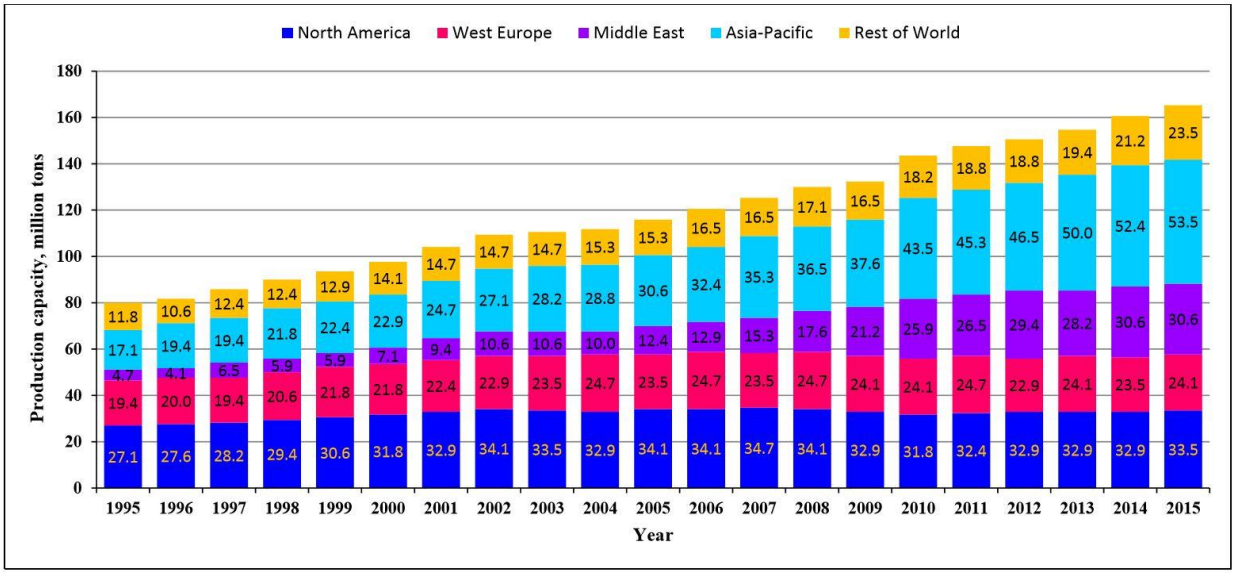

Figure 2. Ethylene capacity growth region wise over the years [2].

1.2 Sources of Ethylene

Natural gas (ethane) and naptha are the main sources of ethylene production. We can see their distribution in Figure 3 [2, 7]. We can see from the Figure 3 that, however naptha is the major feedstock for ethylene production but share of ethane has gradually increased. The cost of feedstock accounts for 60-80% of ethylene production costs. The main factors driving feedstock price changes for petrochemical plants and price of oil and natural gas. In natural gas-rich regions, ethane was the main feedstock for the

ethylene production in recent years [2]. Infact, ethylene feedstock was more profitable than LPG and naptha.

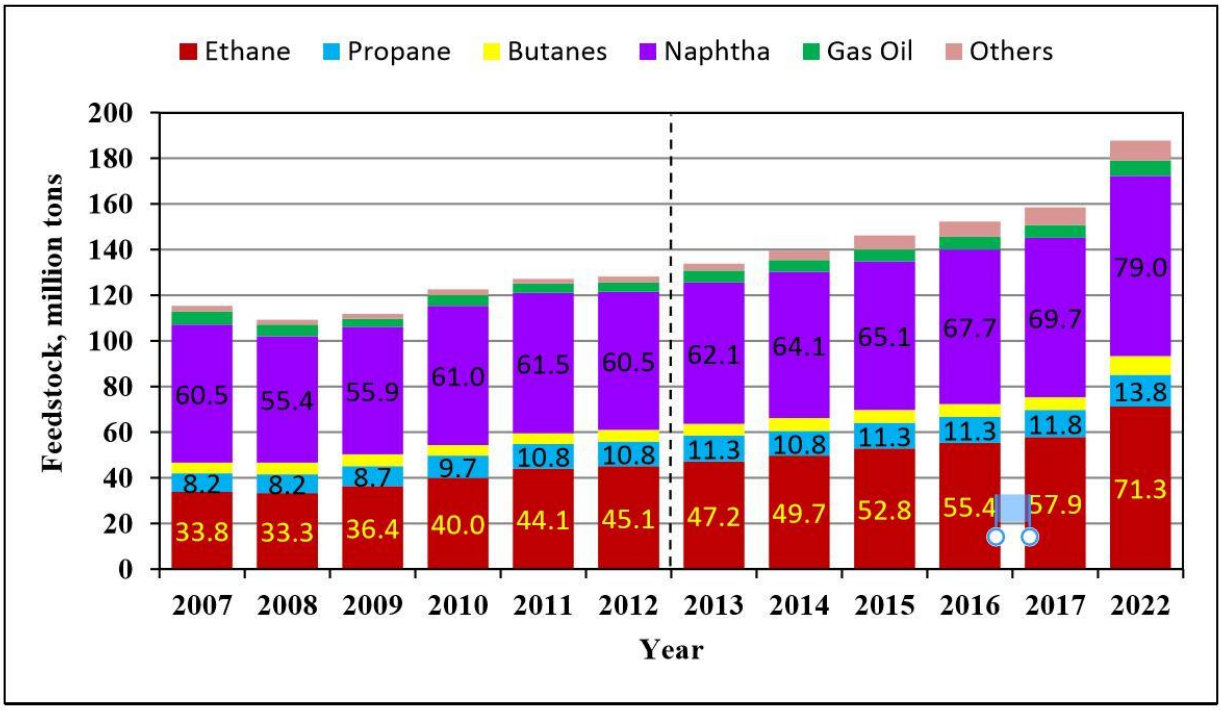

Figure 3. Ethylene production over the years by Feedstock [2].

1.3 Methods of Ethylene Production

Tube furnace pyrolysis has been the main technology for ethylene production over the years and has also improved over the course of several decades. Almost 99% of global ethylene production uses tube furnace pyrolysis method. Figure 4 shows the flow diagram for the pyrolysis [2]. First pre-heated hydrocarbon feedstock (500 to 680 ^{o}C) is mixed up with dilution steam in the convection zone and then it was quickly discharged to the radiation zone (750 to 875 ^{o}C). where the feed is cracked to produce ethylene

and other small olefins. The residence time for the whole process is 0.1 to 0.5 seconds. To curb further side reactions, the high temperature effluent has to be quenched within 0.02 to 0.1 seconds in the transfer line exchanger. Using ethane as feedstock, hydrocarbon conversion of ~70% was achieved and olefin yield of ~50% was obtained [8].Single pass conversion and yield are lower in naptha crackers.

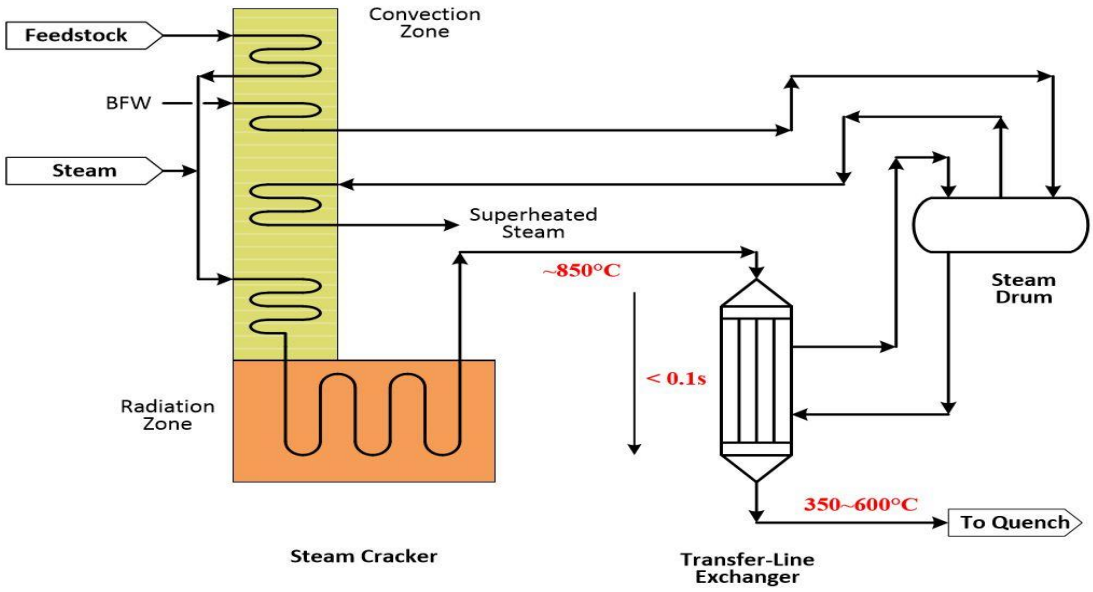

Figure 4. Steam Cracking Process [2].

1.4 Thesis Objective

In this study, we performed catalytic dehydrogenation of ethane known as ethane dehydrogenation (EDH) reaction. We used a MFI-type zeolite membrane with 1wt% Pt/Al_2O_3 catalyst to study the effect of operating conditions on the EDH reaction at high temperatures between 500 to 600 ^oC. MFI zeolite membranes has small pore size which helps in selectively removing hydrogen from the product side and

thus shifting the equilibrium towards the product side. Moreover, because the EDH reaction is endothermic, the reaction is favored at high temperatures for obtaining high ethane conversion, high activity, and high ethylene selectivity and zeolite membranes have high hydrothermal stability which is needed for the EDH reaction. In addition, a one dimensional (1D) plug flow reactor (PFR) model is established for the zeolite packed bed membrane reactor (PBMR). The model is validated and used to simulate and examine the dependencies of EDH PBMR performance upon the operating conditions. The model was further used to investigate the effect of operating conditions beyond the experimental conditions.

Chapter 2

Background and Literature Review

2.1 Zeolites and Zeolite Membranes

Zeolites are microporous aluminosilicate minerals made up of tetrahedral. In the tetrahedral one atom is either Si or Al, which is surrounded by four oxygen atoms. These tetrahedral are linked to each other by common oxygen atom which gives cavities to the structure with definite size and shape [9]. For completely siliceous materials, the framework is electrically neutral. There are more than 170 types of zeolite structures that have been identified so far. Then supported polycrystalline zeolite membranes are suitable for energy efficient separation of gas and liquid mixtures [10]. Macroporous and mesoporous ceramic, stainless steel,glass plates and tubes are some common membrane supports mostly in the form of disc and tubes [11-13]. Many types of zeolites membranes have been tested for various molecular separations[14-16].The pore sizes of 8-member ring LTA ,10-member ring MFI and 12-member ring FAU are about 0.41, 0.56 and 0.74 nm, respectively. These are most extensively studied structures because their pore sizes are suitable for separating a large number of chemicals important for chemical industry.

Zeolites membranes are commonly synthesized by hydrothermal treatment of the substrate surface in liquid phase aluminosilicate precursor which can be in the form of clear solution, sol or gel. The crystallization of zeolites and eventual crystal structure are sensitive to the precursor composition, the use

of structure directing agents (SDA), the specific route of precursor preparation, and the synthesis temperature and duration. Undesirable impurity crystal phases, present in zeolite films, can affect the morphology, impurity and chemical stability [17].

The general process for the synthesis of polycrystalline zeolite membranes on porous substrate is shown in Figure 5. In an in-situ crystallization process, zeolite nuclei form on the surface either by heterogeneous nucleation or by deposition of nuclei generated in the bulk solution. While in the seeded secondary growth method, the zeolite seed layer, is pre coated using separately synthesized zeolite suspensions. The discrete layer of nuclei or seed crystals subsequently evolves in a continuous film by crystal growth in a synthesis solution. The final zeolite membrane consists of inter grown-crystals with minimized intercrystalline spaces. These intercrystalline spaces are considered as microdefects because they are larger than the zeolite pores and decrease molecular separation selectivity [18].

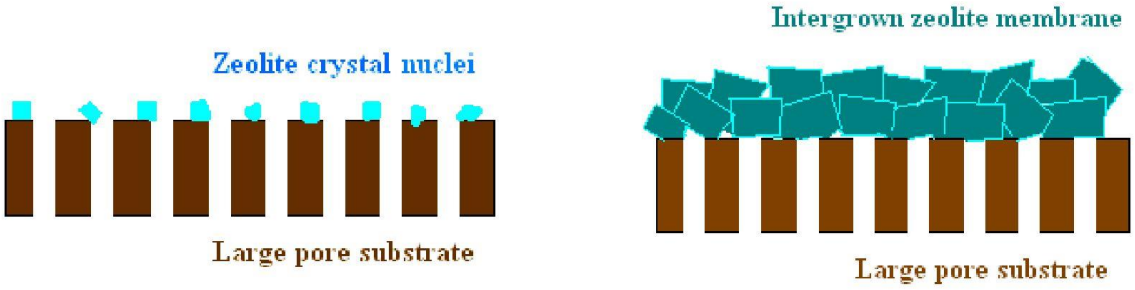

Figure 5. Schematic description of zeolite membrane formation on a porous substrate(a) nucleation on surface and (b) crystal growth in to continuous polycrystalline membrane [19]

2.2 Zeolite membrane reactors

Membrane reactors (MR) selectively removes one of the product which helps it in achieving better performance than Traditional reactor (TR). MR are economical as they can perform separation and reaction in a single step. Due to growing importance of H_2, active work has been performed in the recent past to develop H_2 selective membranes [20-22].Overall MR reactor has three main advantages over TR: (1) It can help in achieving higher conversion than equilibrium conversion obtained from thermodynamic limitations, (2) MR can achieve same conversion as TR but at milder operating conditions, and (3) It also reduces the capital and operating costs due to combination of reaction and separation in one step.

Uniform pore size, crystalline structure and well defined pore systems make zeolite membranes promising for the EDH reactions. The application of zeolite membrane for EDH reaction depends upon the ability to fabricate zeolite membrane with high selectivity, high permeance, good hydrothermal stability, strong chemical resistance and low cost [23, 24].

Required catalyst volume for a certain conversion is less for MR than TR [25]. High thermal and mechanical strength of MFI-type zeolite membrane enables it to be operated at high temperature and high pressure [26, 27].Thus high temperature and high pressure operation with MFI-type zeolite membrane in MR mode causes substantial decrease in operating cost.

2.3 Review for EDH

In recent years, several studies have been done for EDH reaction. For example, Galvita et al. [3] reported experiments for an EDH traditional reactor using catalysts of Pt-Sn/Mg(Al)O and Pt/Mg(Al)O. The conversion values reported were 4.3% and 9.8%, respectively, which were substantially less than the

equilibrium limit of 16% at 600 °C. Sun et al. [28] proposed an approach for preparing a catalyst for EDH reaction by dispersing Pt nanoparticles onto a calcined hydrotalcite support containing In and Al, Mg(In)(Al)O. The activity of Pt/Mg(In)(Al) was found to be a strong function of the bulk In/Pt ratio. The maximum catalyst activity of 29 μmol s^{-1} $gcat^{-1}$ and ethylene selectivity of 98% was achieved at a In/Pt ratio of 0.48. Gudgila et al. [29] studied oxidative ethane dehydrogenation reaction (OEDH) over Pt catalyst and investigated the effect of alumina, silica, and zirconia support on packed bed reactor (PBR) performance. Ethane conversion of 75% was quite similar for all three supports, but ethylene yield was maximum as 46% for silica support followed by alumina support and zirconia support. Wu et al. [30] investigated the effect of Sn as a promoter with Pt catalyst on EDH reaction. Catalyst deactivation due to coke formation was found to be strongly affected by catalyst particle size and Sn/Pt ratio. Deactivation decreased substantially on decreasing particle size and increasing addition of Sn. Hakonsen et al. [31, 32] studied OEDH at short contact times over Pt-Sn monoliths. Catalysts prepared from different impregnation procedures were tested for OEDH. Catalysts prepared by co-impregnation, where Pt is impregnated first and then Sn, appeared to be more beneficial than the one in which Sn is impregnated first and then Pt. For ethane conversion of 40%, selectivity of ethylene was 90% for the former case but was only 86% for the latter one.

Because the equilibrium limit exists in traditional PBR, packed bed membrane reactors (PBMR) became an important subject to explore because they can combine chemical reaction and separation in one step. Membrane is selective to only one of the products which helps in shifting the equilibrium towards the forward reaction, and PBMR is able to overcome the equilibrium limitations and eventually exceed ethane conversion in PBR. For example, Gobina and Hughes [33-36] used a Pd–Ag membrane supported on a vycor glass tube to perform EDH membrane reactor experiments using ethane/N_2 as a feed gas mixture and Pt/Al_2O_3 as a catalyst. For PBMR, ethane conversion of 18%, which was much higher than the equilibrium

conversion of 3.5%, and ethylene selectivity close to 100% were reported. Szegner. et al. [37] reported EDH PBMR with composite alumina membrane with Pt-Sn/Al_2O_3. The ethane conversion of 16% in the PBMR was higher than that of 8% in the PBR and ethylene selectivity of the PBMR was 99% at 550 ^oC. Zhengnam et al. [2] used natural modernite as the membrane and Pt/Al_2O_3 as the catalyst for studying EDH reaction. Ethane conversion and ethylene selectivity were improved from 4.8% and 92.4% for PBR to 5.5% and 94.8% for PBMR, respectively, at 500 ^oC. Lobera et al. [5] used solid state oxygen permeable material ($Ba_{0.5}Sr_{0.5}Co_{0.8}Fe_{0.2}O_{3-i}$) for EDH PBMR. Ethylene was selectively produced by avoiding the direct contact of molecular oxygen and hydrocarbons. Methane was used as an almost-inert dilutant to reduce oligomerization and aromatization of formed ethylene which further helped in improving reactor stability even at 900 °C. Ahchieva et al. [38] studied the performance of a fluidized bed membrane reactor (FLBMR) in comparison with a fluidized bed reactor (FLBR) for catalytic oxidative dehydrogenation of ethane. The effect of temperature and contact time on performance was investigated. FLBMR outperformed FLBR substantially and the reported yield for FLBMR was 37%.

Therefore, reports have addressed that PBMR overcomes the equilibrium limit existing in PBRs. However, reports on high temperature EDH PBMR have been so far very limited. Recently, the MFI zeolite membrane reactors were successfully tested for high-temperature catalytic reactions of 400-500 ^oC [14, 39-43]. Due to good hydrogen selectivity of MFI-type zeolite membrane, high thermal and mechanical strength of MFI-type zeolite membrane and ability of the MR to combine separation and reaction in one step, the MFI-type zeolite membranes could be promising candidates for EDH as PBMR.

Chapter 3

Synthesis of MFI type zeolite membranes

3.1 Preparation of membranes

The MFI zeolite membrane was synthesized on a seeded α-alumina disk by secondary growth. Macroporous α-alumina disks (Coorstek) of 1 in. diameter, 1 mm thickness, and 25% porosity were used as supports for MFI zeolite membrane preparation. Details of polishing α-alumina disks prior to membrane growth are identical to those described previously [39, 44]. To prepare a seeded α-alumina disk, the MFI seeds were dip-coated on the α-alumina supports, dried, and calcined using the same procedures described elsewhere [39, 40]. The synthesis solution was prepared as follows: tetrapropylammonium hydroxide (TPAOH, 1 M, Sigma–Aldrich) was mixed in deionized water. After 30 min of stirring, tetraethyl orthosilicate (TEOS, 98%, Acros) was added dropwise to the solution under constant stirring. The molar composition of the gel was TEOS: 0.095 TPAOH: 35.42 H_2O. After the precursor was stirred for 3 h, it was transferred into the Teflon-lined stainless steel autoclave (Parr). The polished α-alumina disk was placed vertically at the bottom of the vessel and completely immersed in the synthesis solution. The synthesis experiments were performed at 150 ^oC for 17 h. After the hydrothermal reaction, the membrane was washed thoroughly with deionized water, dried, and calcined in air at 550 ^oC for 6 h to remove the template. The membranes were dried at 70 ^oC in an oven overnight.

3.2. Membrane Properties

3.2.1 Membrane Performance Parameters

The membrane was tested for permeation of equimolar H_2/C_2H_6 and H_2/C_2H_4 mixtures in a temperature range of room temperature to 600 °C. The membrane permeance for gas component *i* is defined as

$$P_{m,i} = \frac{Q_i}{A_m \cdot \Delta P_i}, \qquad (i = H_2, C_2H_6, \ldots) \tag{1}$$

where Q_i (mol/s) is the amount of gas permeated over a time period of *t* (*s*); A_m (m^2) is the active membrane area which is 2.01 cm^2 excluding the area sealed by the graphite gasket; and ΔP_i (Pa) is the transmembrane pressure, $\Delta P_i = (P_i)_f - (P_i)_p$, where $(P_i)_f$ and $(P_i)_p$ are the partial pressures of *i* in the feed and permeate sides, respectively. The H_2/C_2H_6 perm-selectivity ($a^o_{H2/C2H6}$) is defined as the ratio of pure gas permeance:

$$\alpha^o_{H2/C2H6} = \frac{P_{m,H2}}{P_{m,C2H6}} \tag{2}$$

The H_2/C_2H_6 separation factor ($\alpha_{H2/C2H6}$) for the binary mixture is given by

$$\alpha_{H2/C2H6} = \frac{(y_{H2} / y_{C2H6})_{permeate}}{(y_{H2} / y_{C2H6})_{feed}} \tag{3}$$

where y_{H2} and y_{C2H6} are mole fractions of H_2 and C_2H_6, respectively.

3.2.2. Zeolite membrane properties

Fig. 6 shows the SEM micrographs of the surface and cross section of the secondary grown zeolite membrane. The membrane showed well-intergrown polycrystalline films and the thickness of the zeolite layer was ~7 μm.

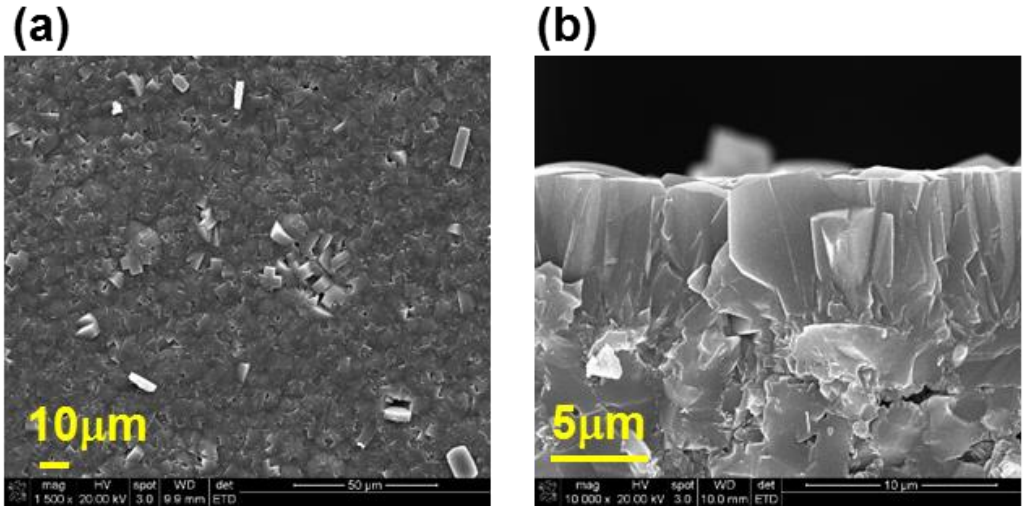

Figure 6. SEM images of the secondary grown zeolite MFI membranes: (a) surface and (b) cross section.

Moreover, as shown in table 1, the reproducibility of the secondary growth method was very good. The deviations of H_2 gas permeance and H_2/CO_2 separation factor of the individual membranes obtained under same conditions were within ±3% and ±8%, respectively. Thus, M4 was used in this study. As shown, the reproducibility of membrane synthesis was > 90%, meaning that nine out of ten membranes obtained by secondary growth exhibited gas permeation properties within the above deviation ranges.

Table 1. H_2/CO_2 separation factor variation at room temperature for different zeolite membrane

Membrane	H_2/CO_2 separation factor at 25 °C
M1	0.88
M2	0.86
M3	0.83
M4	0.81

In Fig. 7a, the MFI-type membranes were evaluated for separation of an equimolar H_2/C_2H_6 mixture over a temperature range of 23 - 600 °C to determine their applicability in EDH membrane reactors. At 23 °C, the fresh MFI membrane was selective toward C_2H_6 with a H_2/C_2H_6 separation factor of 0.46 and a low H_2 permeance of 9.3×10^{-9} mol m^{-2} s^{-1} Pa^{-1} because the preferentially adsorbed C_2H_6 limited the access of H_2 molecules to the zeolitic pores. As temperature increased, diffusion became predominant and the membrane experienced a transition from being C_2H_6-selective to H_2-selective at ~135 °C. At 600 °C, H_2/C_2H_6 selectivity ($\alpha_{H2/C2H6}$) increased from 0.46 to 3.31 and the H_2 permeance was enhanced from 9.3×10^{-9} to 1.2×10^{-7} mol m^{-2} s^{-1} Pa^{-1}, both of which are consistent with the behavior expected from MFI membranes. Fig. 7b presents the H_2/C_2H_4 separation results monitored during the entire separation process, and H_2/C_2H_4 selectivity ($\alpha_{H2/C2H4}$) increased from 0.46 to 3.00. During the separation, the H_2 permeances were enhanced from 1.3×10^{-8} to 1.3×10^{-7} mol m^{-2} s^{-1} Pa^{-1}.

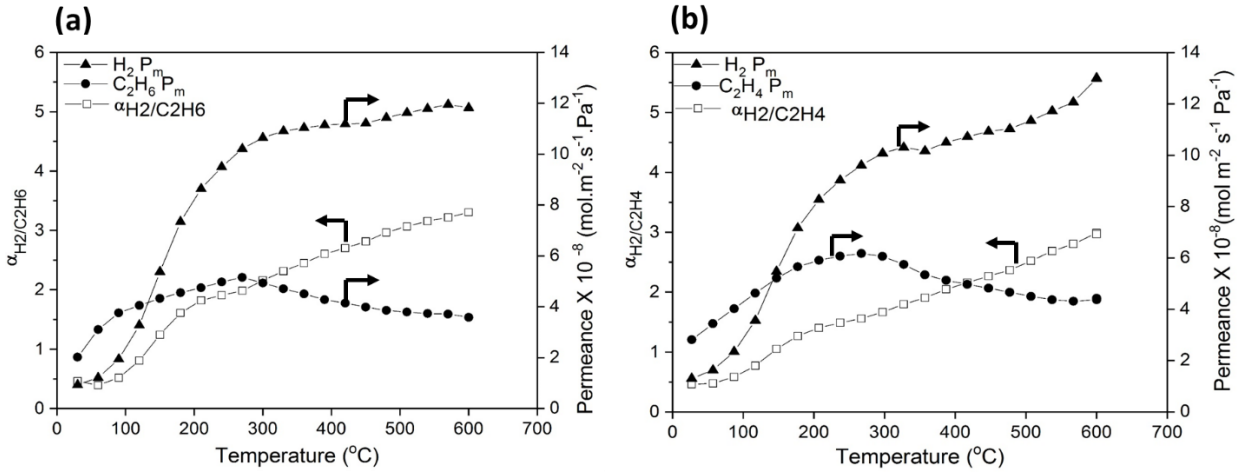

Figure 7. Permeation characteristics of (a) H_2/C_2H_6 and (b) H_2/C_2H_4 equimolar mixtures in MFI zeolite membranes as a function of temperature.

Moreover, H_2/C_2H_4 separation factor and $P_{m,H2}$ were measured before and after the membrane was used in EDH membrane reactors (Fig. 8). After EDH membrane reaction experiments that lasted about ~200 h, the H_2/C_2H_4 separation factor showed increase of 10% and $P_{m,H2}$ at 600°C showed increase of 12%, respectively. One possible reason might be the deposition of coke on membrane pores which caused increase in H_2 permeance and decrease in ethylene permeance and thus increase in separation factor. Thus, it can be concluded that the membrane performance was stable during long term EDH reaction (> 200 h) and there are no significant structural changes affecting performance. Table 2 shows the change in performance parameters for the H_2/C_2H_4 mixture before and after the EDH reaction.

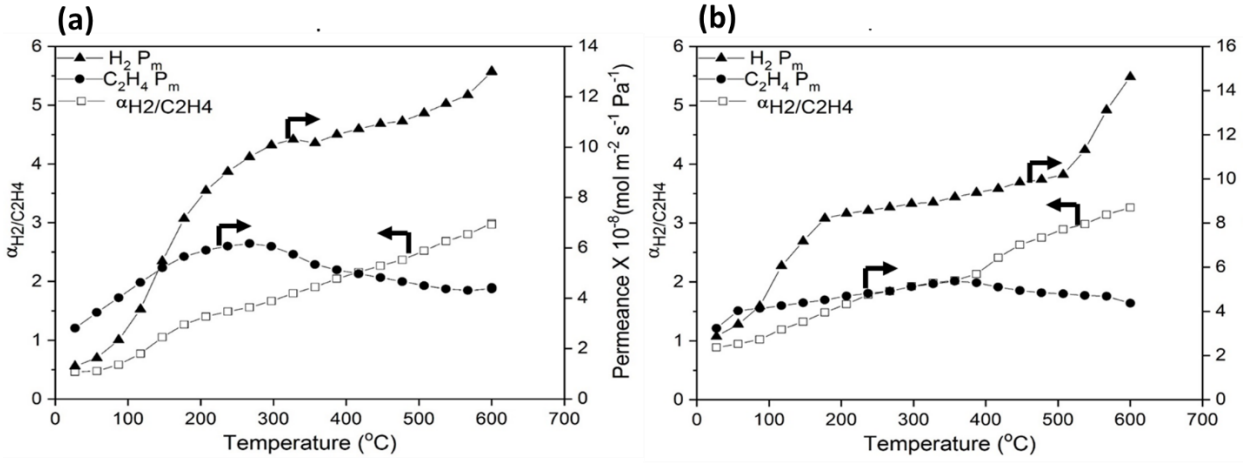

Figure 8. Permeation characteristics of H_2/C_2H_4 (a) before EDH experiment and (b) after EDH experiment for equimolar mixtures in MFI zeolite membranes as a function of temperature.

Table 2. Separation properties for H_2/C_2H_4 equimolar mixture before and after the EDH reaction

	Before Reaction at 600 °C	**After Reaction at 600 °C**	**Deviation (%)**
S/F	2.97	3.26	10
P_m $H_2 \times 10^{-8}$ (mol/s.m^2.Pa)	13.01	14.62	12
P_m Ethylene $\times 10^{-8}$ (mol/s.m^2.Pa)	4.42	4.37	1

3.3. Summary

MFI type zeolite membrane was synthesized by secondary growth method on a seeded macroporous α-alumina disk of 1 in. diameter, 1 mm thickness, and 25% porosity. The synthesis solution had the composition of TEOS: 0.095 TPAOH: 35.42 H_2O. The synthesis experiments were performed at 150 ^oC for 17 h. Eventually membrane was dried, and calcined in air at 550 ^oC for 6 h to remove the template. SEM pictures showed well-intergrown polycrystalline films with the thickness of the zeolite layer was ~7 μm. The membrane was tested for separation of an equimolar H_2/C_2H_6 and H_2/C_2H_4 mixture over a temperature range of 23 - 600 °C to determine their applicability in EDH membrane reactors. The H_2/C_2H_6 and H_2/C_2H_4 separation factor increased from 0.46 at 23 °C for both the mixture to 3.31 and 3.0 at 600 °C. The corresponding increase in the permeance value was from 9.3×10^{-9} to 1.2×10^{-7} mol m^{-2} s^{-1} Pa^{-1} for H_2/C_2H_6 and from 1.3×10^{-8} to 1.3×10^{-7} mol m^{-2} s^{-1} Pa^{-1} for H_2/C_2H_4.

Chapter 4

High Temperature EDH Reaction in microporous Zeolite Membrane Reactor

4.1 Experimental

4.1.1 EDH reaction

The EDH membrane reactor system is schematically shown in Fig. 9. The disc membrane was mounted in a stainless steel cell sealed by soft graphite gaskets (Mercer Gasket & Shim). A total amount of 550 mg of Pt/Al_2O_3 catalyst was spread evenly over the membrane surface to form a uniform catalyst bed. A thin pad of carbon cloth and quartz wool was placed on top of the catalyst layer to fix the catalyst bed and allow for feed gas to diffuse freely. The permeate side was swept by Ar flow at atmospheric pressure and its flow rate was maintained at 20 cm^3/min for all experiments, except for those which focus on the effect of F_{Ar}. The flow rates of ethane and Ar were controlled by mass flow controllers (MFC, Aalborg).

The flow rate of the exit stream from the reactor (retentate and permeate) was frequently checked by soap bubble tests.Preheating coils were employed for both the feed and sweep gases to ensure that they reached the set temperature before entering the reactor. The retentate and permeate gases were analyzed by an online GC (Shimadzu GC2014) equipped with a molecular sieve 13X column for the thermal conductivity detector (TCD) and an alumina plot column for the flammable ionization detector (FID). The flow rate checked by soap bubble tests was multiplied by the gas composition (obtained from GC) to find the individual gas flow rate in the exit stream. In the inlet flow rate for each gas is maintained by MFC. A

heating and cooling rate of 0.5 ^{o}C/min was used. The ethylene product, unreacted ethane, H_2, and the byproducts (methane, propylene, xylene, and benzene) from side reactions, such as thermal cracking and catalytic cracking, were analyzed to observe the influence of operating conditions on reaction conversion and selectivity. Minor byproducts such as higher alkanes and higher olefins (propylene and butylene) and aromatics (benzene, xylene, and toluene) were found to be far less than 1% and excluded from further consideration. The ethane conversion was calculated based on the total ethane feed flow rates entering as feed and exiting the reactor in both the permeate and retentate streams:

$$\chi_{C2H6} = 1 - \frac{F_{C2H6}^{out}}{F_{C2H6}^{in}} \tag{4}$$

The selectivity for gas component *i* is defined as:

$$S_i = \frac{F_i^{out} - F_i^{in}}{F_{C2H6}^{in} - F_{C2H6}^{out}} \qquad (i = C_2H_4, CH_4 \ldots) \tag{5}$$

The yield for gas component *i* is calculated by:

$$Y_i = \frac{\chi_{C2H6} \times S_i}{100} \qquad (i = C_2H_4, CH_4 \ldots) \tag{6}$$

The weight hourly space velocity (WHSV) is defined by:

$$WHSV = \frac{\upsilon_{feed}^{C2H6} \times \rho_{C2H6}}{m_{cat}} \tag{7}$$

where υ_{feed}^{C2H6} is the volumetric rate of ethane in the feed stream at standard temperature and pressure (STP), and m_{cat} is the mass of catalyst. The catalyst used in the PBMR and PBR experiments was 1% Pt/Al_2O_3

(Sigma Aldrich) denoted here as 'Pt/Al_2O_3' catalyst. When the membrane-mounted cell was used in PBR mode, the entering sweeping gas was removed and the exit of the reaction side was connected to the original sweeping inlet. The gas stream from the reaction side thus passed through the permeate chamber to exit from the permeate side. The EDH operating conditions are in Table 3. The reaction being highly endothermic becomes feasible above 400 °C so the temperature ranges of 500-600 °C was chosen. Moreover, higher ethane flow rate means higher space velocity and lower conversion so ethane flow rate was maintained in such a way that conversion values are in the respectable ranges. For F_{Ar}, a minimum ratio of 2 (F_{C2H6}=10cm^3/min and F_{Ar} =20 cm^3/min) was maintained for F_{Ar} /F_{C2H6} so that there will always be a good enough driving force for H_2 removal towards the permeate side.

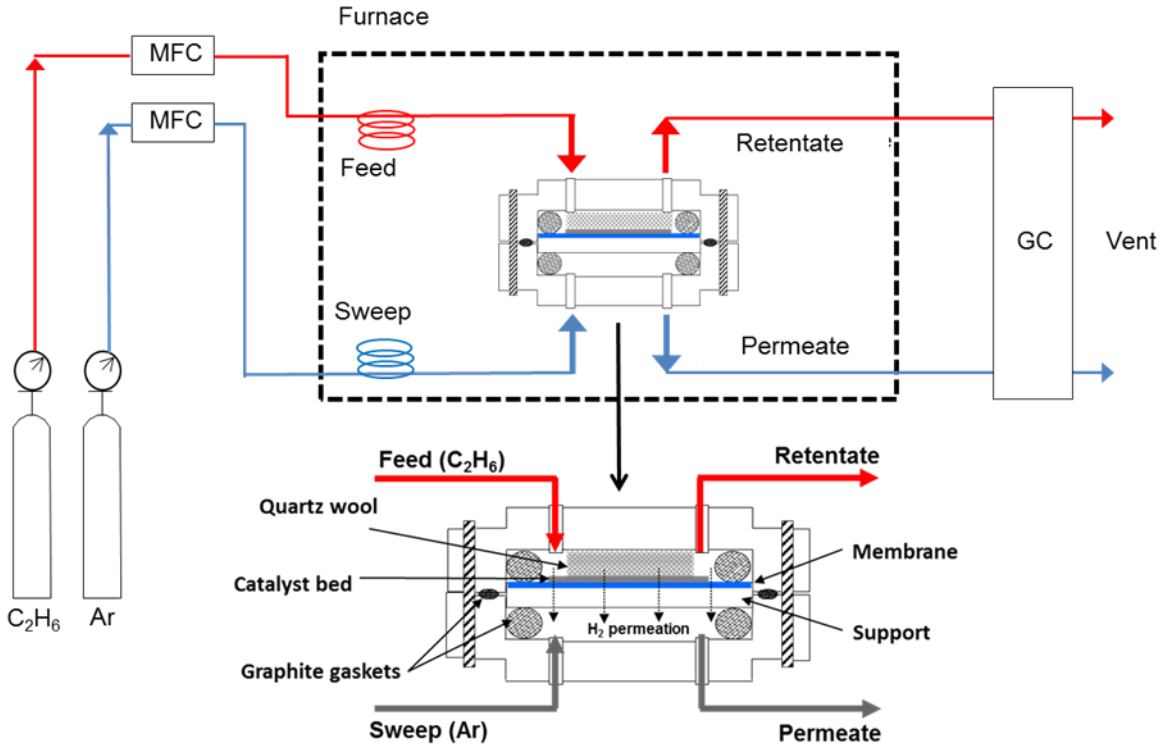

Figure 9. Schematic diagram showing membrane reactor system used for EDH reaction.

Table 3. EDH membrane reactor conditions

Reaction temperature, °C	500 - 600
Weight hourly space velocity (WHSV), h^{-1}	0.3 - 1.5
C_2H_6 feed flow rate, F_{C2H6}, cm^3 (STP)/min	2 - 10
Ar sweeping flow rate, F_{Ar}, cm^3 (STP)/min	0 - 30
1% Pt/Al_2O_3 catalyst loading (m_{cat}), g	0.55
Reactor pressure at retentate exit, atm	1.0
Permeate pressure, atm	1.0

4.2. Results and Discussions

4.2.1. Effect of reaction temperature

The MFI-type zeolite PBMR was first examined for EDH reactions at 500 - 600 °C with pure ethane as a feed, Ar sweeping flow rate (F_{Ar}) of 20 cm^3/min, and WHSV of 0.45 h^{-1}. The results of the EDH PBMR reaction are presented in Fig. 10 in comparison with the PBR operation mode. As temperature was increased, the rate of reaction also increased and more products were formed at a faster speed. As more products were formed, the ethane conversion increased for both PBR and PBMR with temperature. However, from Fig. 10 it might seem that ethane conversion increases linearly with temperature but we suggest it would be too far-fetched to conclude that from the three data points. The nature of the ethane conversion with temperature may change in anyway on further increasing the temperature. The error bars in Fig. 10a and 10b shows the deviation in ethane conversion and ethylene selectivity. The maximum deviation was 6% in ethane conversion and 3% in ethylene selectivity. In the PBMR, due to selective

permeation of H_2, EDH reaction shifted towards the product side, which led to a more enhanced ethane conversion than the equilibrium limit.

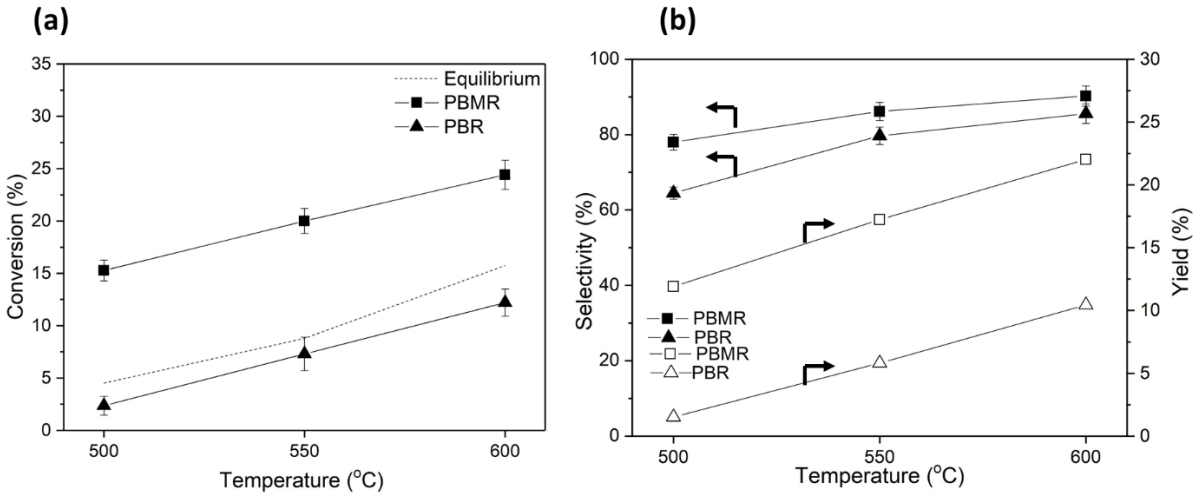

Figure 10. Effect of reaction temperature on (a) ethane conversion, and (b) ethylene selectivity and ethylene yield, in PBMR and PBR (WHSV = 0.45 h^{-1}; F_{Ar} = 20 cm^3/min; and p_{perm} = 1 atm).

Moreover, the EDH reaction became faster with increasing temperature, which led to enhanced ethylene selectivity. In the PBMR, there is less H_2 in the feed side which may lead to less hydrogenolysis and thus the selectivity of ethylene for the PBMR is higher than the PBR. It can be seen that the introduction of H_2 selective MFI-type membrane leads to higher selectivity and yield over the PBR. The PBMR reached ethylene selectivity of 90%, due to its efficient removal of H_2 generated in the EDH reaction and thus increased the overall reaction selectivity toward EDH over the side-reactions.

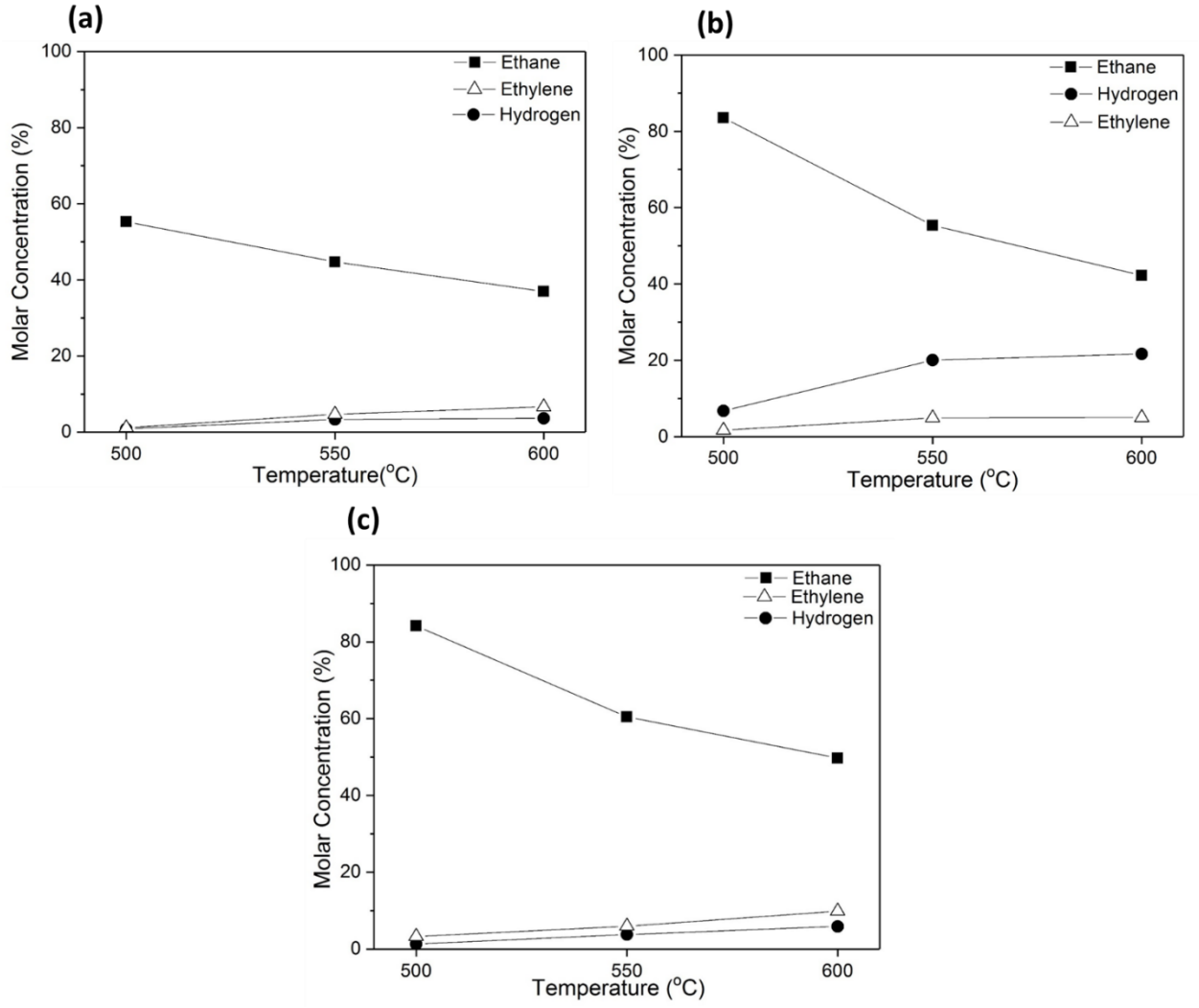

Figure 11. Effect of temperature on molar concentration of ethane, ethylene and H_2 for (a) PBMR retentate, (b) PBMR permeate and (c) PBR. ($WHSV$ = 0.45 h^{-1}; F_{Ar} = 20 cm^3/min; and p_{perm} = 1 atm).

Fig. 11 presents the molar concentrations of components in the retentate and permeate streams of the PBMR (Fig. 11a and Fig. 11b) and PBR (Fig. 11c). Due to H_2 removal through the MFI membrane, the H_2 molar concentration in the retentate stream of the PBMR was notably lower than that in the PBR. Also the permeate stream of the PBMR has a higher H_2 molar concentration in comparison to the PBR. Ethane molar

concentration for PBMR retentate stream is lower than PBR. This is because of the selective permeation of H_2 across the membrane which results in higher ethane conversion in PBMR than PBR.

4.2.2. Effect of space velocity

Fig. 12 presents the results of EDH reaction in PBMR and PBR at 600 °C and WHSV of 0.3 - 1.48 h^{-1}. WHSV is defined as the number of reactor volumes which can be processed in per unit time. As WHSV increases, the reactants spend less time inside the reactor, which leads to lower ethane conversion.

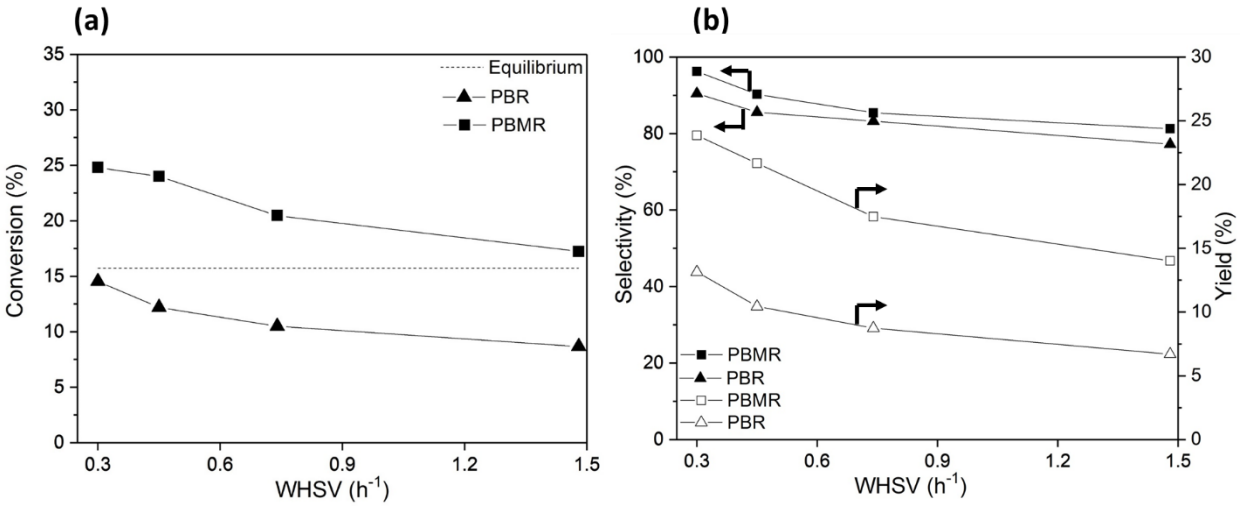

Figure 12. Effect of WHSV on (a) ethane conversion, and (b) ethylene selectivity and ethylene yield, in the PBMR and PBR (temperature = 600 °C; F_{Ar} = 20 cm^3/min; and p_{perm} = 1 atm).

The ethane conversion in the PBMR increased with decreasing WHSV due to the longer residence time for reaction and H_2 permeation at smaller WHSV. The MFI membranes achieved ethane

conversion of 24% and ethylene selectivity of 90% at 600°C and WHSV of 0.45 h^{-1} while the PBR showed ethane conversion of 12% and ethylene selectivity of 86%. The ethylene selectivity and yield of the PBMR and PBR also decreased with an increase in WHSV, but the PBMR had higher ethylene selectivity and yield than PBR due to selective removal of H_2.

4.2.3. Effect of sweep flow

The use of a sweep gas on the permeate side is desirable to increase the driving force for the H_2 permeation rate. Fig. 13 shows the ethane conversion and ethylene selectivity at 600°C and WHSV of 0.45 h^{-1}, as a function of F_{Ar}, which was varied in the range of 10 - 30 cm^3/min.

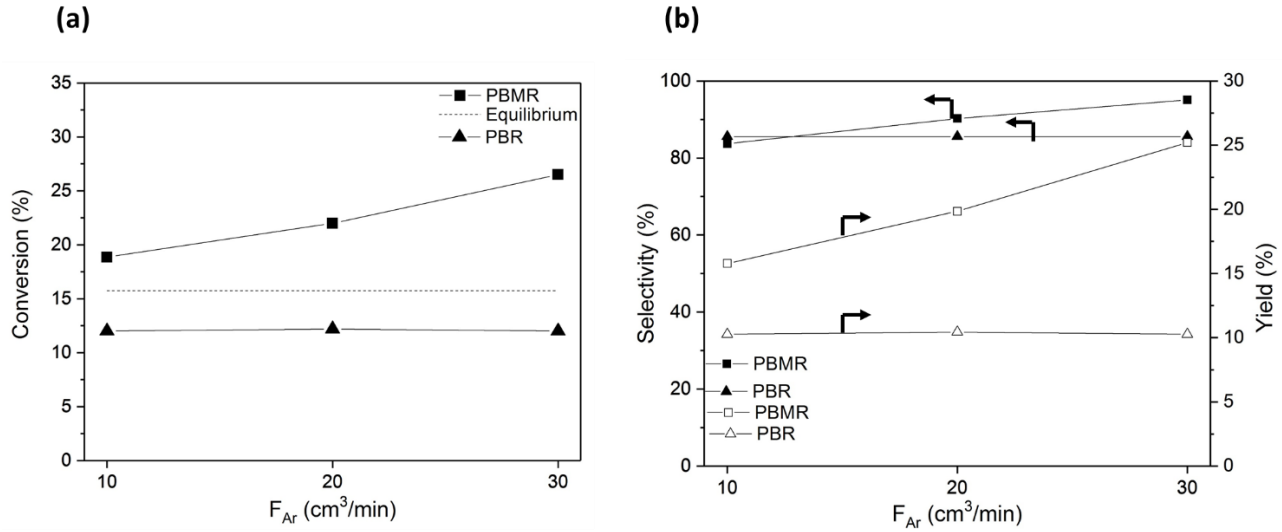

Figure 13. Effect of F_{Ar} on (a) ethane conversion, and (b) ethylene selectivity and ethylene yield, in PBMR and PBR (temperature = 600 °C; WHSV = 0.45 h^{-1}; and p_{perm} = 1 atm).

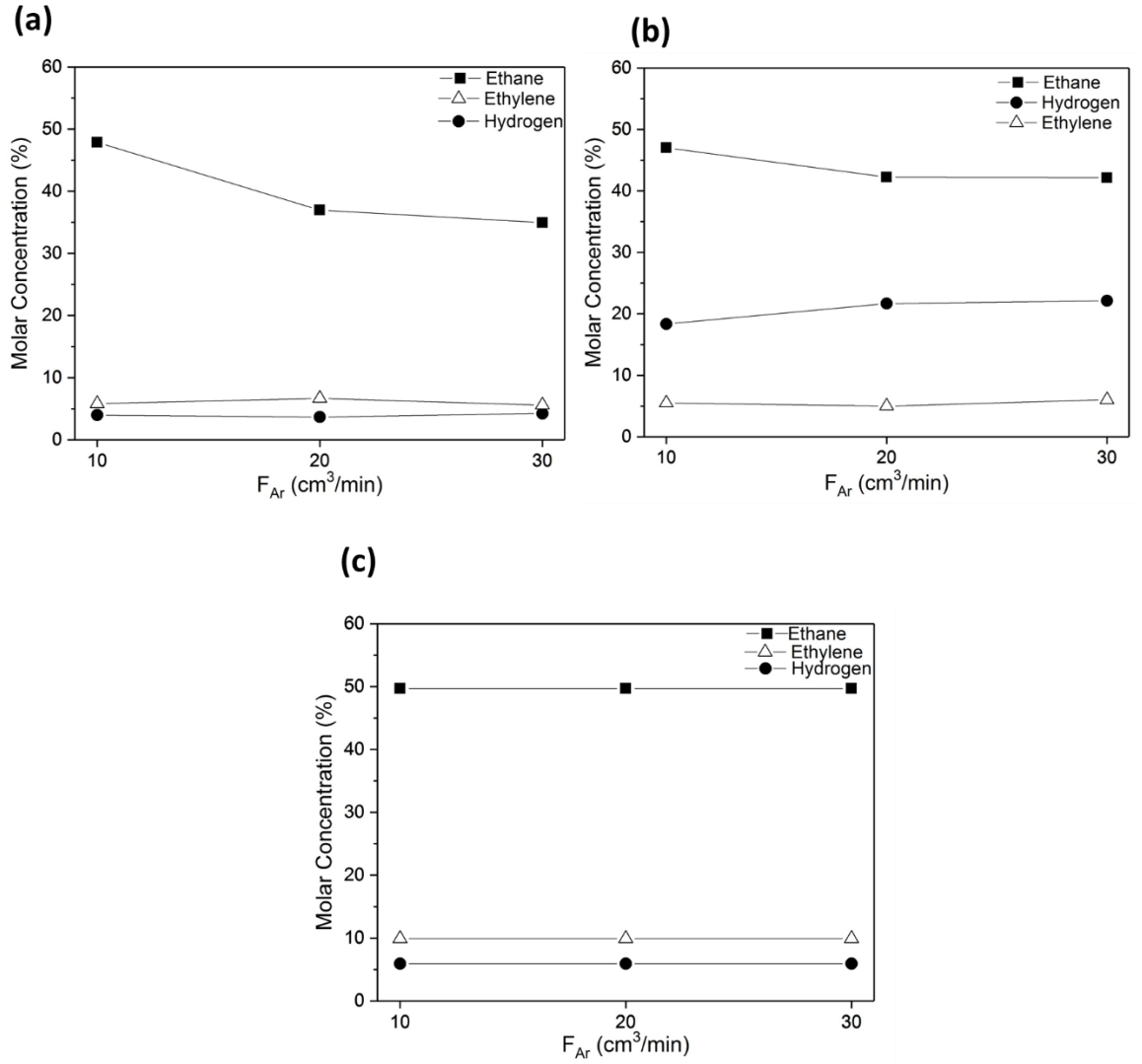

Figure 14. Effect of F_{Ar} on molar concentration of ethane, ethylene and H_2 for (a) PBMR retentate, (b) PBMR permeate and (c) PBR (temperature = 600 °C; *WHSV* = 0.45 h^{-1}; and p_{perm} = 1 atm).

The ethane conversion, ethylene selectivity, and ethylene yield of the PBMRs were found to be all strong functions of F_{Ar}. Increasing F_{Ar} reduced the permeate H_2 partial pressure and hence increased

the H_2 permeation driving force and membrane flux, thereby enhancing the ethane conversion. When F_{Ar} was further increased from 30 to 40 cm^3/min, the PBMR performance characteristics leveled off at much higher levels than the PBR performance. When the output concentration from the reactor was analyzed by online GC, it was found that at lower $F_{Ar,}$ H_2 permeation values were smaller than rate of H_2 formation rate from the reaction therefore on increasing F_{Ar} more H_2 permeates even more and ethane conversion increases with F_{Ar}. But with increasing F_{Ar}, the H_2 permeance and external mass transport resistances were no longer the rate-limiting step for enhanced conversion. The rate of ethane conversion by the catalyst at the given WHSV began to limit the PBMR performance and therefore the conversion value levels off when F_{Ar} was increased from 30-40 cm^3/min. In all cases, it is noteworthy that the PBMR significantly outperformed the PBR. As discussed earlier, it can be seen in Fig. 14.

4.2.4. Methanation

Methane is one of the main byproducts in the EDH reaction. Methanation reaction is endothermic and therefore high temperature favors the methanation reaction [45]. The selectivity of methane was examined for both PBR and PBMR operation modes at 500-600 °C. The WHSV and F_{Ar} were fixed at 0.45 h^{-1} and 20 cm^3/min. The amount of methane in both permeate and retentate was examined by GC. Fig. 15 shows the comparison of methane selectivity between PBR and PBMR operations. As expected, methane selectivity increased with increasing temperature for both PBR and PBMR [46-49]. The methane selectivity increased from 3.2% to 8.7% for PBMR while for PBR, the increase was from 7.6% to 12.8%. The low methane selectivity in PBMR operation can be attributed to the removal of H_2, a reactant for methane formation. Low methanation selectivity in PBMR is an important advantage over PBR as PBMR removes useful H_2 and creates less methane impurity.

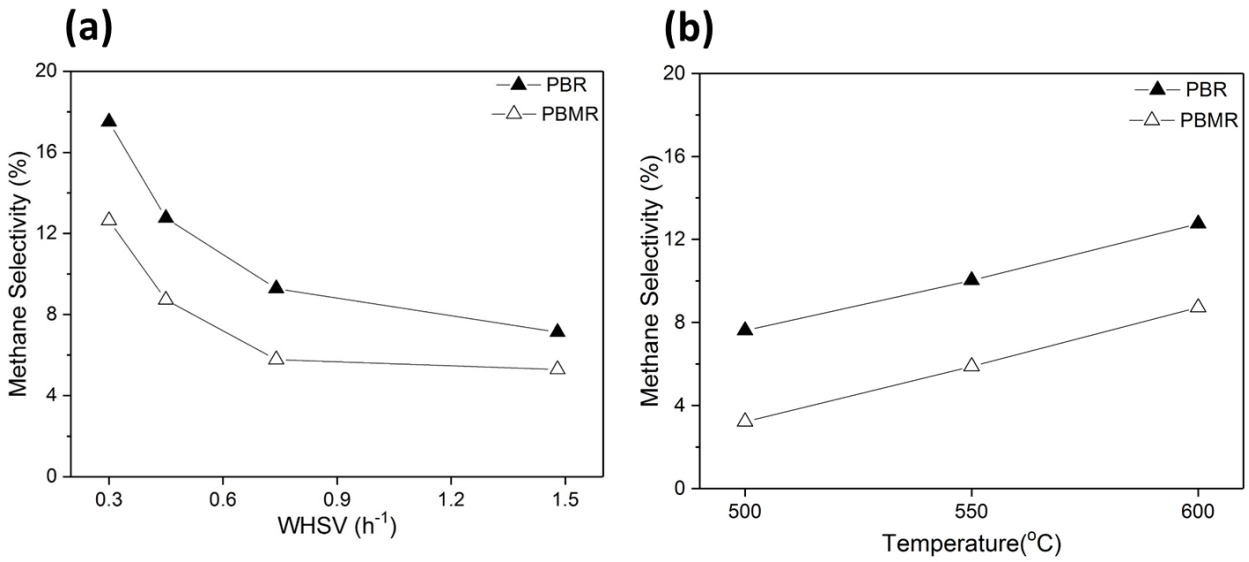

Figure 15. Effect of (a) WHSV on methane selectivity and (b) temperature on methane selectivity for PBR and PBMR for (temperature = 600 °C; WHSV = 0.45 h^{-1}; and F_{Ar} = 20 cm^3/min).

4.2.5. Effect of H_2 addition in the feed

In all the experiments, a catalyst deactivation has been observed, which leads to a rapid decrease in catalyst activity in the first hour after EDH reaction started. Catalyst deactivation and regeneration are important considerations for alkane dehydrogenation processes. Some dehydrogenation technologies use H_2 as a feed diluent to reduce coking and elongate catalyst lifetime between regeneration cycles. (a) H_2 is considered to inhibit the formation of coke because it reduces the concentration of coke precursors (light hydrocarbons such as ethylene and propylene), which can form the oligomers and carbonaneous compounds. (b) We have evaluated this aspect in the context of the PBR and PBMR.

Figure 16a-c shows the influence of H_2 concentration in the feed on the ethane conversion, ethylene selectivity and ethylene yield. All the values shown in this study were taken after one hour when the steady state was ensured and there was almost no change in outlet composition. The ethane conversion and ethylene selectivity decreased as H_2 concentration in the feed is increases. When H_2 is used in the feed there is more H_2 in the reaction side which leads to shift the dehydrogenation reaction towards the reactant side and thus lesser conversion. Moreover, when there is more H_2 hydrogenolysis reaction also becomes important and thus selectivity of ethylene also decreases with increase in H_2 concentration in feed. However, ethane conversion and ethylene selectivity values for the PBMR were higher than PBR as expected.

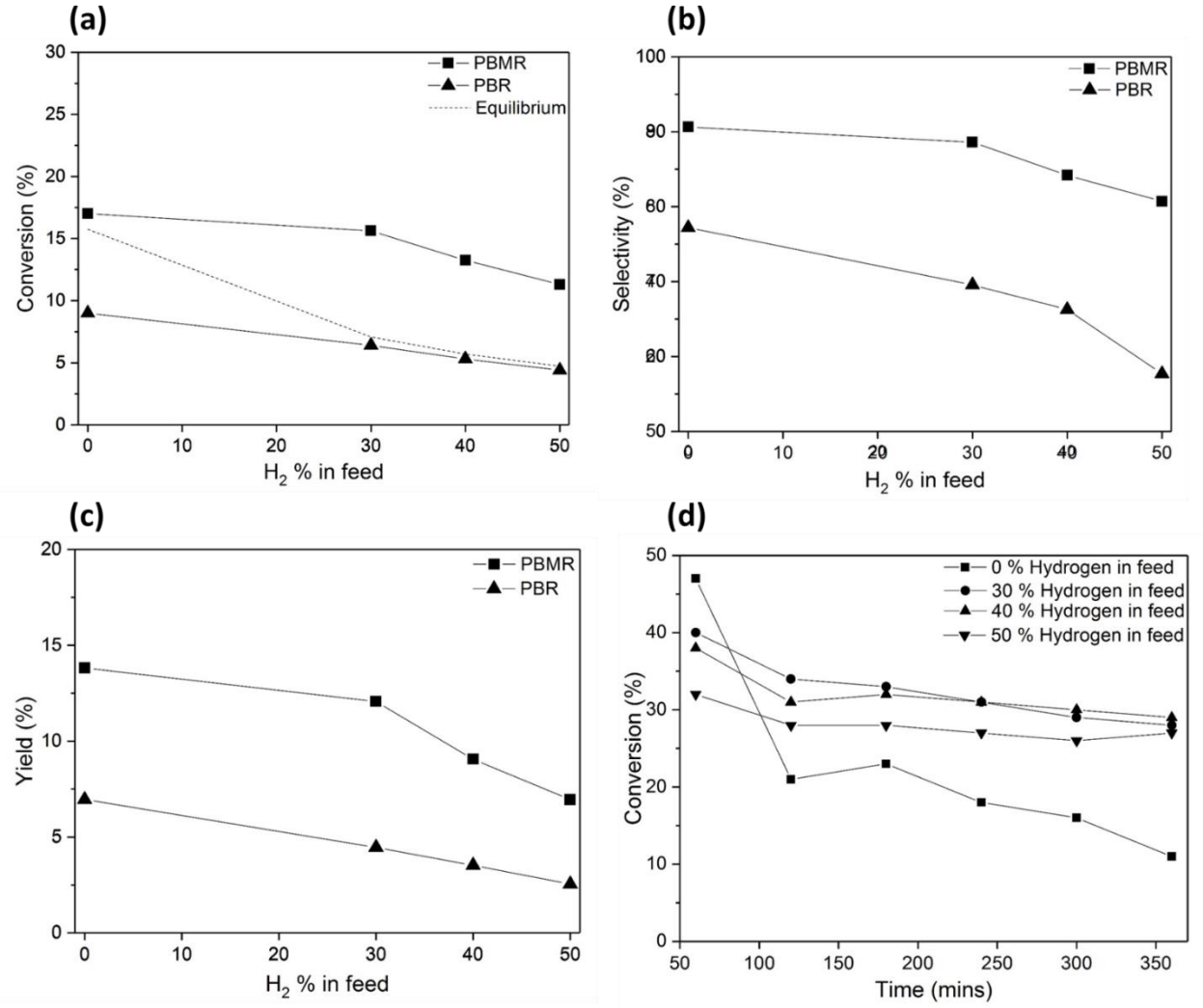

Figure 16. Effect of H_2 concentration in feed on (a) ethane conversion (b) ethylene selectivity (c) ethylene yield, and (d) conversion of ethane with time for Temperature of 600 °C and WHSV of 0.45 h^{-1} for feed (50% ethane and 50% H_2)-10 cm^3/min

As shown in Figure 16d, in the absence of H_2, both conversion and the selectivity significantly decline with increasing time-on-stream. This is due to catalyst deactivation, which occurs via deposition of carbonaceous matter (generated by undesired side reactions such as propylene cracking) on the active

surface of the catalyst. However, the addition of H_2 provides a much more stable time-dependence of the catalyst activity and selectivity up to 350 mins of EDH, albeit with an initially lower conversion than with a pure hydrocarbon feed. PBR and PBMRs showed the similar trends of propane conversion and propylene selectivity. The initial lower conversion is probably because an increase in H_2 partial pressure not only decrease the thermodynamic driving force but also increase the competitive adsorption of H_2 with ethane on the catalyst. [46-49]

4.3. Summary

The disc membrane was mounted in a stainless steel cell sealed by soft graphite gaskets and a total amount of 550 mg of Pt/Al_2O_3 catalyst was used to form a uniform catalyst bed. The flow rate of the exit stream from the reactor was frequently checked by soap bubble tests. The retentate and permeate gases were analyzed by an online GC (Shimadzu GC2014) equipped with a molecular sieve 13X column for the thermal conductivity detector (TCD) and an alumina plot column for the flammable ionization detector (FID). The aim of the study is to study the impact of different operating conditions (temperature, F_{Ar} and WHSV) on reaction performance parameters (ethane conversion, ethylene selectivity and ethylene yield). EDH PBMR showed higher ethane conversion, ethylene selectivity and ethylene yield than EDH PBR because of selective removal of H_2 from the reaction to the permeate which helped in shifting the equilibrium to the forward reaction. With increase in temperature ethane conversion increases because the reaction occurs at a faster pace at high temperature which leads to more product. While for space velocity the effect was reverse, with increase in WHSV ethane conversion decreases because the reactant spends less time in the reactor. Moreover, the effect of sweep gas was also studied. With increase in the F_{Ar} the ethane conversion, ethylene selectivity and ethylene yield increases because the driving force for the H_2

permeation increases (as H_2 partial pressure in permeate side decreases) which helps in shifting the equilibrium towards the product side. Finally, H_2 was used in the feed to study its impact on the catalyst stability. However, all these enhancements in values of ethane conversion, ethylene selectivity and ethylene yield for PBMR in comparison to PBR came when all the operating conditions were same which means there was no extra investment in terms of energy to achieve this enhancement in performance and just the introduction of membrane helped in achieving this enhancement in performance parameters. Without hydrogen catalyst activity was drastically decreased in the first hour. But when hydrogen was used in the feed, it inhibits the coke formation due to which there was not substantial decrease in the catalyst performance. However, there was a decrease in ethane conversion in presence of H_2 which was expected as H_2 is a product.

Chapter 5

Modeling and Simulation of High Temperature EDH Reaction in MFI Zeolite Membrane Reactor

5.1 Model for EDH MR Simulation

5.1.1. Kinetic Equations

The EDH reaction is endothermic as shown in

$$C_2H_6 \leftrightarrow C_2H_4 + H_2,\ \Delta H^{\Theta}_{298.15K} = \ 136.94\ kJ/mol \tag{8}$$

The following rate expression was used for modelling and taken from reference. [37]

$$Rate = k\left(P_{ethane} - \frac{P_{ethylene} \times P_{hydrogen}}{K_{Eq}} \right) \tag{9}$$

The kinetic rate constant and equilibrium constants have been studied in the literature. [45, 50]

$$k = k_0 \exp\left(\frac{-E}{RT}\right) \tag{10}$$

$$K_{eq} = 7.28\times10^{6} \exp\left(\frac{-17000}{T+273}\right) \tag{11}$$

where R is the universal gas constant, k is the rate constant and K_{eq} is the equilibrium constant. The activation energy (E) and rate constant (k_0) for the system are 20.6 kcal mol^{-1} and 0.00423 mol m^{-2} s^{-1} Pa^{-1} [37, 40, 51-53]. The reference we choose to take the values of activation energy and rate constant also used the same catalyst for the EDH reaction so we assumed that the catalyst morphology and substrate interactions will not bring significant changes. The aim of the modelling is to investigate the effects of reactor operating conditions and zeolite membrane properties on ethane conversion and find the most optimized reaction conditions.

Various assumptions made in the modelling are made for reactor modeling, including (i) isothermal steady state operation, (ii) ideal gas behavior and pressure-independent permeance, (iii) negligible side reactions, and (iv) negligible mass-transfer resistance in the thin catalyst layer (~ 760 μm thick) and the macroporous substrate. The model was validated by comparing with experimental results and then it was used to evaluate the PBMR performance beyond the experimental conditions. Plug flow reactor (PFR) model was used for reactor modeling, which considers both reaction (feed) side and permeate side under plug - flow conditions. Fig. 17 shows the schematic diagram of the membrane reactor structure and concurrent cross flow arrangement used in both experiments and model calculations.

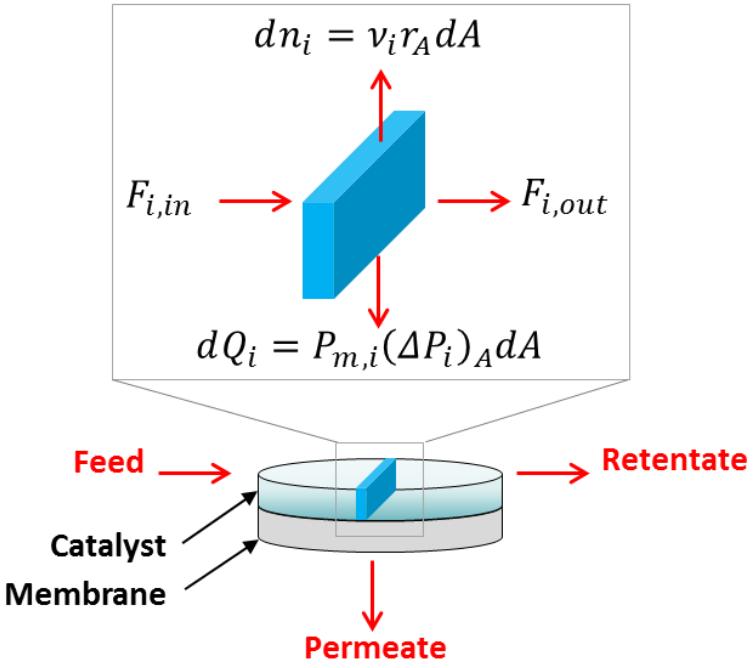

Figure 17. Schematic showing the gas flow arrangement and mass balance in the PBMR.

The 1D PFR model was considered and the mass balance equation for a differential section of the reactor is given by the following equations:

$$dF_i = F_i\big|_{A+dA} - F_i\big|_A = dn_i - dQ_i \tag{12}$$

$$dn_i = \nu_i r_A dA \tag{13}$$

$$dQ_i = P_{m,i}(\Delta P_i)_A dA \tag{14}$$

where F_i (mol/s) is the molar flow of the feed side, A (m^2) is the membrane area, ΔP_i (Pa) is the pressure difference for component i across the membrane, $P_{m,i}$ (mol $m^{-2} s^{-1} Pa^{-1}$) is the permeance of component i, ν_i is the stoichiometric coefficient of species i, Q_i (mol/s) is the gas flow rate through the membrane, and n_i is

the rate of material generation by reaction (mol/s). The differential equations are solved numerically with the membrane being divided into 150 sections of equal membrane area (i.e. equal amounts of catalyst). By setting $Q_i = 0$, equations (12) and describes the PFR model under PBR operation for the same reactor.

5.1.2. Membrane gas permeance

Table 4 lists the values of $P^o_{m,i}$ and $E_{a,i}$ in eq (15) for gases involved in the EDH reaction together with the gas permeance and H_2 selectivity data at 500 °C. These $P^o_{m,i}$ and $E_{a,i}$ values were obtained through regressions of the permeation data of H_2/C_2H_6 and H_2/C_2H_4 binary mixtures, which were measured in the temperature range of 500 - 600 °C under a feed-side pressure of 1 atm and a permeate-side pressure of 1 atm. The gas permeance data for the MFI membrane was measured in the catalyst packed MR after performing the EDH reaction and gas permeation experiments at > 400 °C for more than 1000 h.

$$P_{m,i} = P^{\,o}{}_{m,i} \exp\left(-\frac{E_{a,i}}{RT}\right) \qquad (i = C_2H_6, C_2H_4, H_2) \tag{15}$$

Table 4. $P^0_{m,i}$ and $E_{a,i}$ values for equation (15) and membrane properties at 500 °C

	H_2	C_2H_4	C_2H_6
P^o_m, 10^{-8}, mol m^{-2} s^{-1} Pa^{-1}	12.9	2.60	2.32
$E_{a,i}$, kJ/mol	0.96	3.49	3.17
P_m, 10^{-8}, mol m^{-2} s^{-1} Pa^{-1}	11.6	4.49	3.79
$\alpha_{H2/i}$	-	2.52	3.06

5.2. EDH MR Simulation

5.2.1 Model validation

The EDH reaction was performed by MFI zeolite membrane under temperature range (500-600 °C), WHSV (0.3 - 1.48 h^{-1}), and F_{Ar} (0 - 30 cm^3/min). The experimental results are compared with 1 D PFR model calculations. Fig. 18 shows the comparison between the experimental and calculated ethane conversion values. The calculated values were very much in agreement with experimental values. The model correctly predicted the ethane conversion values increasing with temperature and F_{Ar} and decreasing with WHSV.

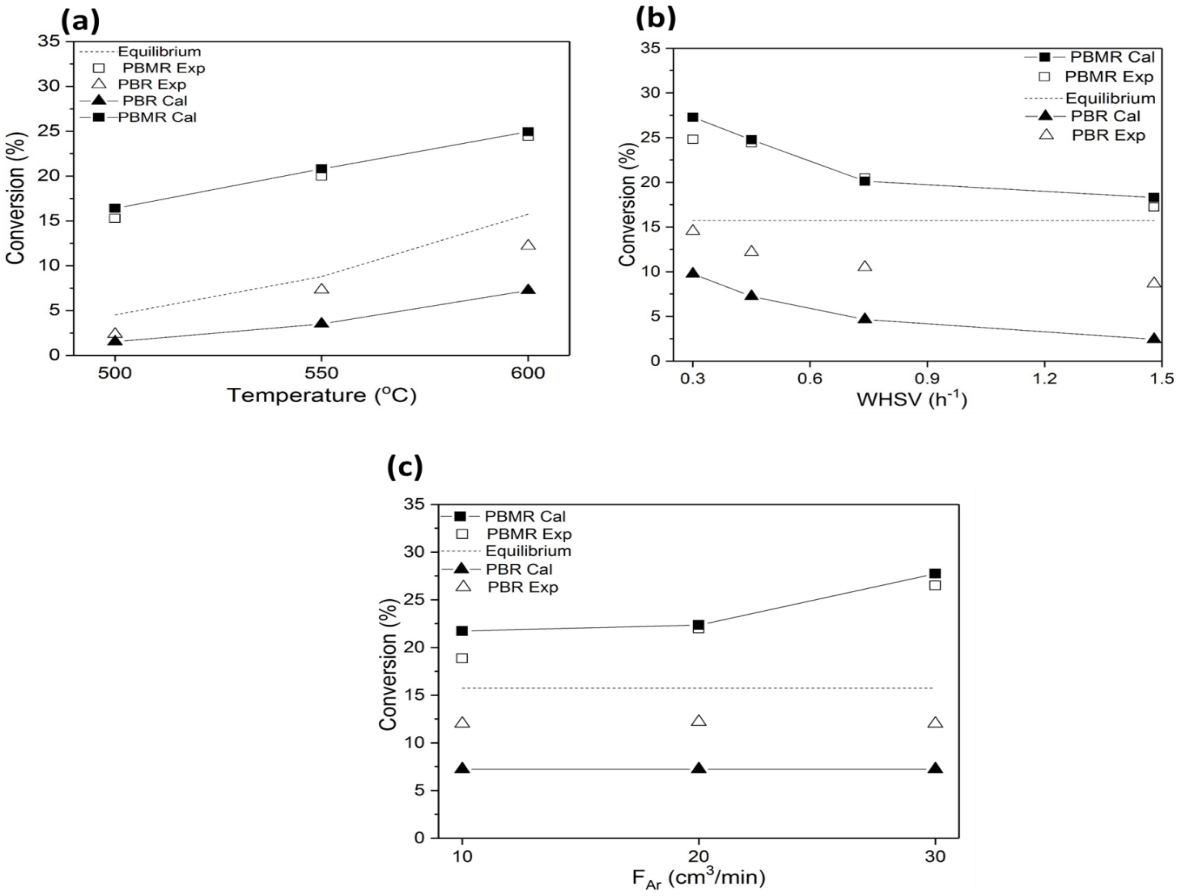

Figure 18. Experimental and simulated ethane conversion for PBMR and PBR as a function of (a) temperature for WHSV = 0.45 h^{-1} and F_{Ar} = 20 cm^3/min and (b) WHSV for 600 °C and F_{Ar} = 20 cm^3/min, and (c) F_{Ar} for temperature = 600 °C and WHSV =0.45 h^{-1}, respectively.

For PBMR, the model slightly overestimated the ethane conversion values. One possible explanation can be the decrease in actual permeance values for ethane, ethylene and H_2 in the experiment as the reaction proceeds, which is not taken into account in the model. In the model calculations, permeance values taken are assumed constant with time for a particular set of conditions and therefore, the actual H_2 permeance may be smaller those that used in the calculations. However, for PBR, the conversion values from the experiment are much higher than those from the model. In the case of PBR, there are substantial side reactions producing multiple by-products such as methane, propane, and propylene. In model calculations, only EDH reaction is assumed, and therefore, the underestimated side reactions may lead to underestimated ethane conversion.

5.2.2 Model calculation

To investigate the possibility for the current membranes to achieve near-complete ethane conversion under practically meaningful conditions, the 1D PFR model was used to simulate the PBMR performance for operations beyond the experimental conditions used in this study. The impact of temperature, feed side pressure, WHSV, and F_{Ar} on ethane conversion were investigated. Operating conditions were temperature of 600 °C, WHSV of 0.45 h^{-1}, feed side pressure (p_{feed}) of 1 atm, and F_{Ar} of 20 cm^3/min unless they were being changed to study their impact.

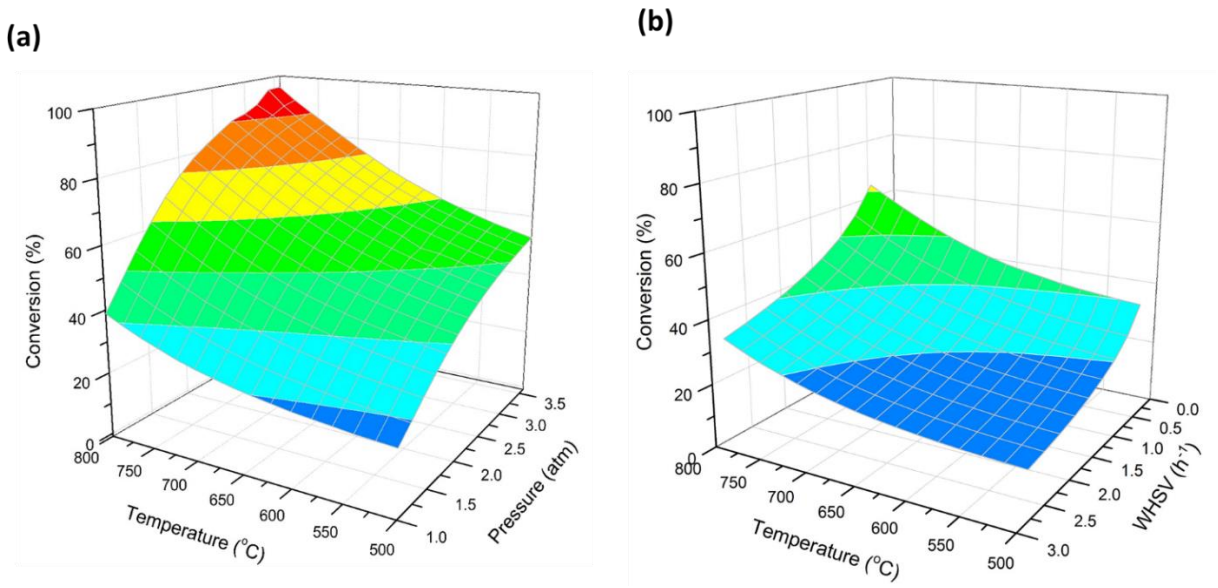

Figure 19. Calculated ethane conversion as a function of (a) the reaction temperature and pressure (WHSV = 0.45 h^{-1} and F_{Ar} = 20 cm^3/min) and (b) the reaction temperature and WHSV (p_{feed} = 1 atm and WHSV = 0.45 h^{-1}), respectively.

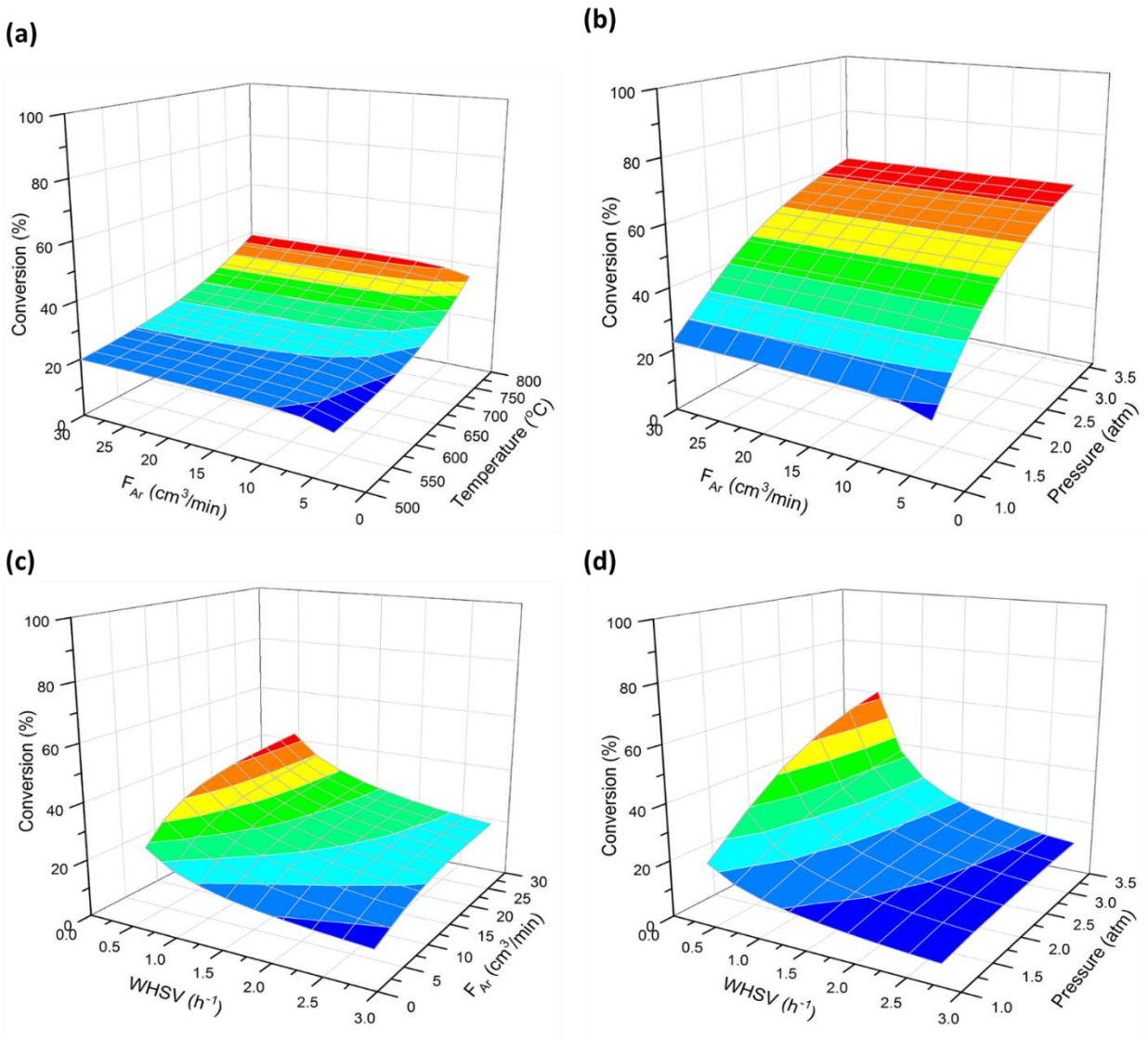

Figure 20. Calculated ethane conversion as a function of (a) temperature and F_{Ar} (p_{feed} = 1 atm and *WHSV* = 0.45 h^{-1}); (b) p_{feed} and F_{Ar} (temperature = 600 °C and *WHSV* = 0.45 h^{-1}); (c) *WHSV* and F_{Ar} (temperature = 600 °C and p_{feed} = 1 atm); and (d) *WHSV* and p_{feed} (temperature = 600 °C and F_{Ar} = 20 cm^3/min) in the PBMR.

Fig. 19 presents the calculated ethane conversion in MFI zeolite membranes as functions of operating conditions. For example, Fig. 19a shows that increasing temperature and p_{feed} both enhance the ethane conversion in the PBMRs. However, the ethane conversion tends to plateau above a certain temperature and pressure. The highest ethane conversion values of 96% in the zeolite PBMR are obtained at T >750 °C and p_{feed} >3.5 atm, which are practically possible conditions. Moreover, Fig. 19b shows the impact of temperature and WHSV on ethane conversion. As expected with increase in WHSV ethane conversion decreases because the reactant spends less time in the reactor. Examples of the other simulation results are given in Fig. 20. The difference in maximum ethane conversion obtained by the PBMR demonstrates the importance of operating conditions. The simulation results indicate that ethane conversion in the PBMR with moderate H_2 selectivity and permeance can be improved significantly by selecting proper operating conditions (i.e., temperature, pressure, WHSV, and F_{Ar}).

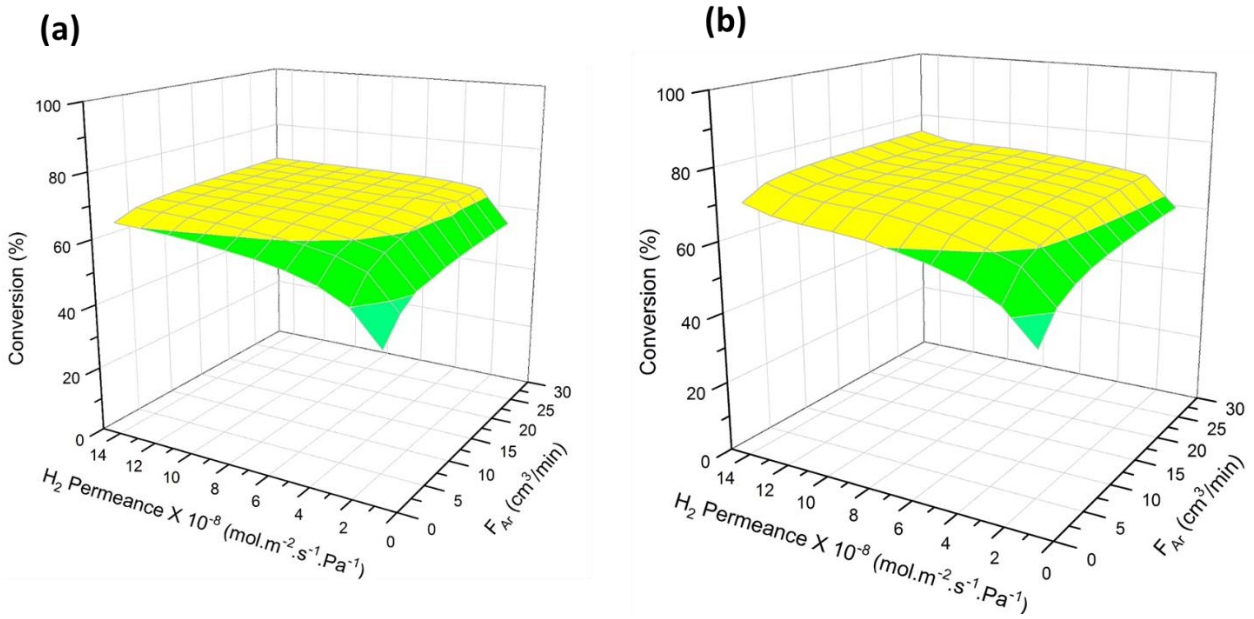

Figure 21. Effect of H_2 permeance (mol m^{-2} s^{-1} Pa^{-1}) and F_{Ar} (cm^3/min) on ethane conversion for WHSV = 0.45 h^{-1} at (a) 500 °C and (b) 650 °C.

As shown in Fig. 21a-b, the results indicate that improving $P_{m,H2}$ for a fixed F_{Ar} helps to enhance the ethane conversion because of the increased permeation of H_2. It is interesting that, for PBMR with a specific $P_{m,H2}$, a maximum ethane conversion appears at a certain level of F_{Ar}, after which further increasing the F_{Ar} causes ethane conversion to level off. Similarly, the plateau of ethane conversion in a PBMR was found with high $P_{m,H2}$ but limited F_{Ar}, and this indicates that the $P_{m,H2}$ is the limiting factor for ethane conversion enhancement. This result suggests that, for a membrane with limited F_{Ar}, a very high $P_{m,H2}$ is not necessarily beneficial for the PBMR performance.

More simulations were carried out to further investigate the feasibility of the current zeolite membrane for achieving the ethane conversion >98%, which is close to the final conversion level of the multiple reactor systems used in the industry. The results have shown that the ethane conversion >98% could be obtained in the MFI zeolite membrane but will require operation conditions beyond those used in the current industrial processes. In this work, the ethane conversion was calculated for zeolite membranes as a function of the reaction temperature and membrane area (A), which corresponds to catalyst loading area for p_{feed} of 1 atm and 1.5 atm. As shown in Fig. 22, the membrane area is given by "A/A_0", where "A" is the membrane used in the calculation and "A_0" is the membrane area used in the experiments (i.e., 0.00020 m^2). It should be noted that the variations of mass transport resistance for different catalyst loads are not considered in the calculations. At different pressure, the ethane conversion increases monotonically as A/A_0 increases. This indicates that the EDH reaction rate as well as membrane separation area are critical factors for the ethane conversion enhancement. An example of the simulation results is given in Fig. 22b at WHSV of 0.45 h^{-1},

and p_{perm} of 1.5 atm. It can be seen that, for the current zeolite membrane, when the membrane area is greater than 0.00031 m^2, the ethane conversion can exceed ~98%. The above simulation results indicate that the ethane conversion in the zeolite PBMR with moderate H_2 selectivity and permeance can be improved significantly by selecting proper operating conditions.

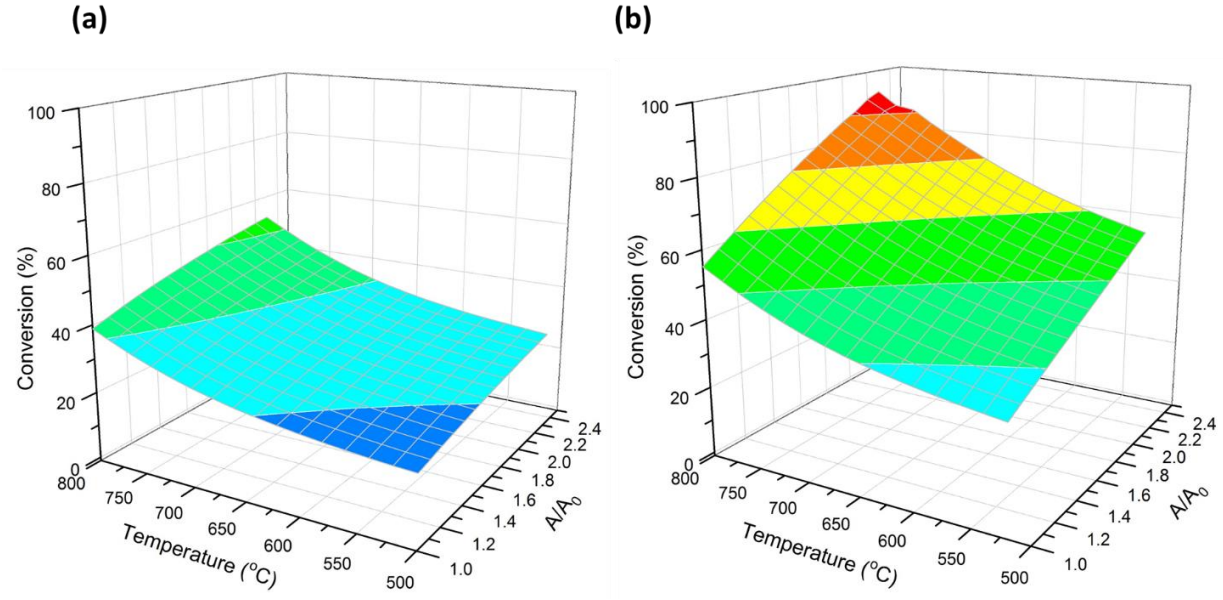

Figure 22. Effect of normalized membrane area (A/A_0) and temperature on ethane conversion for (a) pressure of 1 atm and (b) 1.5 atm (WHSV = 0.45 h^{-1} ; and F_{Ar} = 20 cm^3/min).

Similar simulations were carried out to further investigate the feasibility of the current zeolite membrane for achieving the ethane conversion > 99.5%, which is the final conversion level of the multiple reactor systems used in the industry. The results have shown that the ethane conversion > 99.5% could be obtained in the MFI zeolite membrane but will require operation conditions at elevated pressure. In this work, the ethane conversion was calculated for zeolite membranes as a function of the reaction pressure

(p_{feed}) and membrane area (A), which corresponds to catalyst loading area between 500 to 650 °C. The results of the calculations are shown in Figure 23. In the figure, the membrane area is given by "A/A_0", where "A" is the membrane used in the calculation and "A_0" is the membrane area used in the experiments (i.e., 0.000201 m^2). It should be noted that the variations of mass transport resistance for different catalyst loads are not considered in the calculations. At all temperatures, the ethane conversion increases monotonically as A/A_0 increases. This indicates that the EDH reaction rate as well as membrane separation area are critical factors for the ethane conversion enhancement.

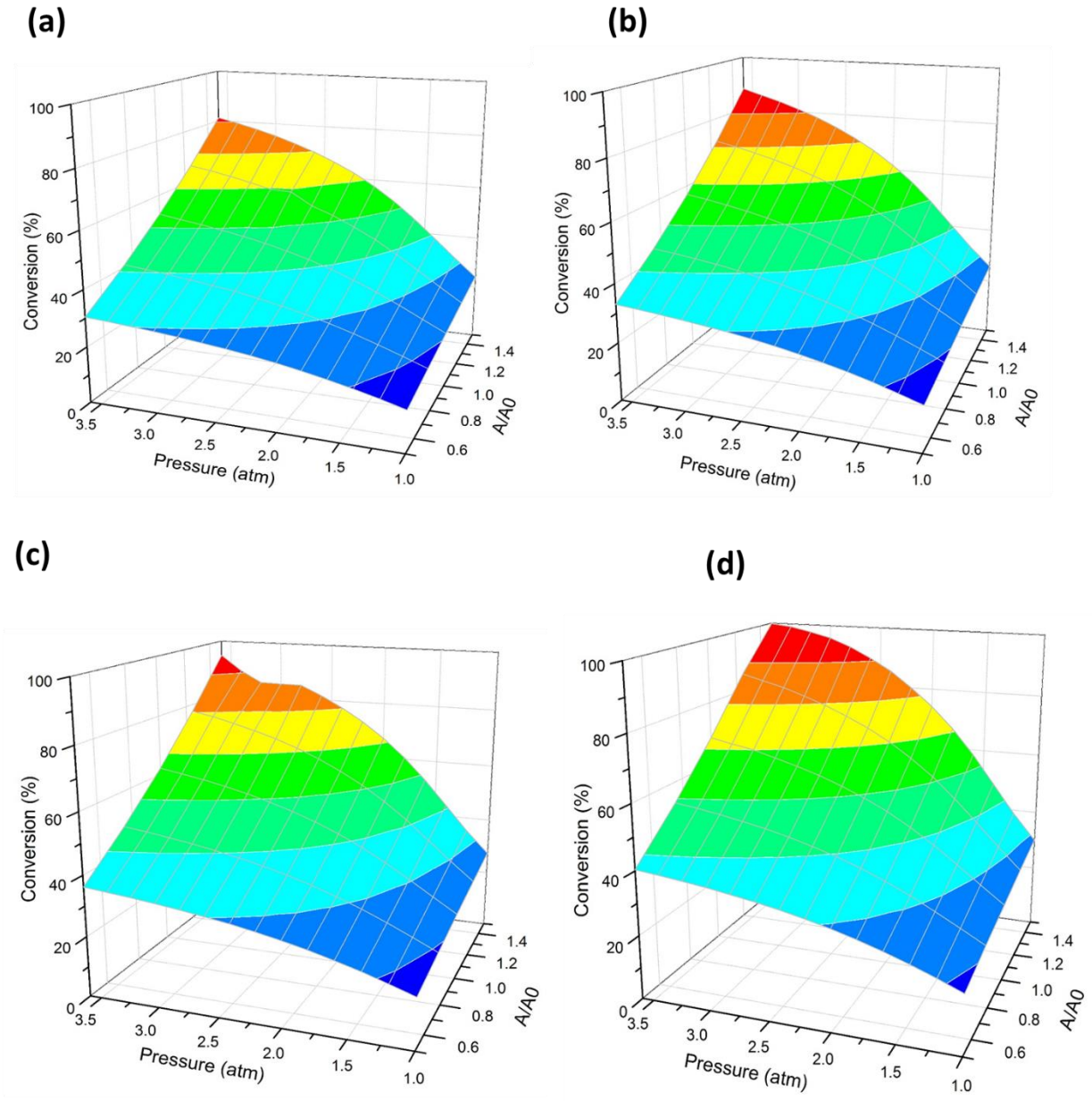

Figure 23. Effect of pressure (atm) and normalized area (A/A0) on ethane conversion for WHSV=0.45 h^{-1} for (a) temperature = 500 °C (b) temperature = 550 °C (c) temperature = 600 °C (d) temperature = 650 °C for feed- ethane 3cm^3/min (100%)

An example of the simulation results is given in Figure 23d at WHSV of 0.45 h^{-1}, and p_{perm} of 1 atm. It can be seen that, for the current zeolite membrane, when the membrane area is greater than 0.000314 m^2, the ethane conversion can exceed 99.5 % under reaction pressures of 3.6 atm. The above simulation results indicate that the ethane conversion in the zeolite PBMR with moderate H_2 selectivity and permeance can be improved significantly by selecting proper operating conditions.

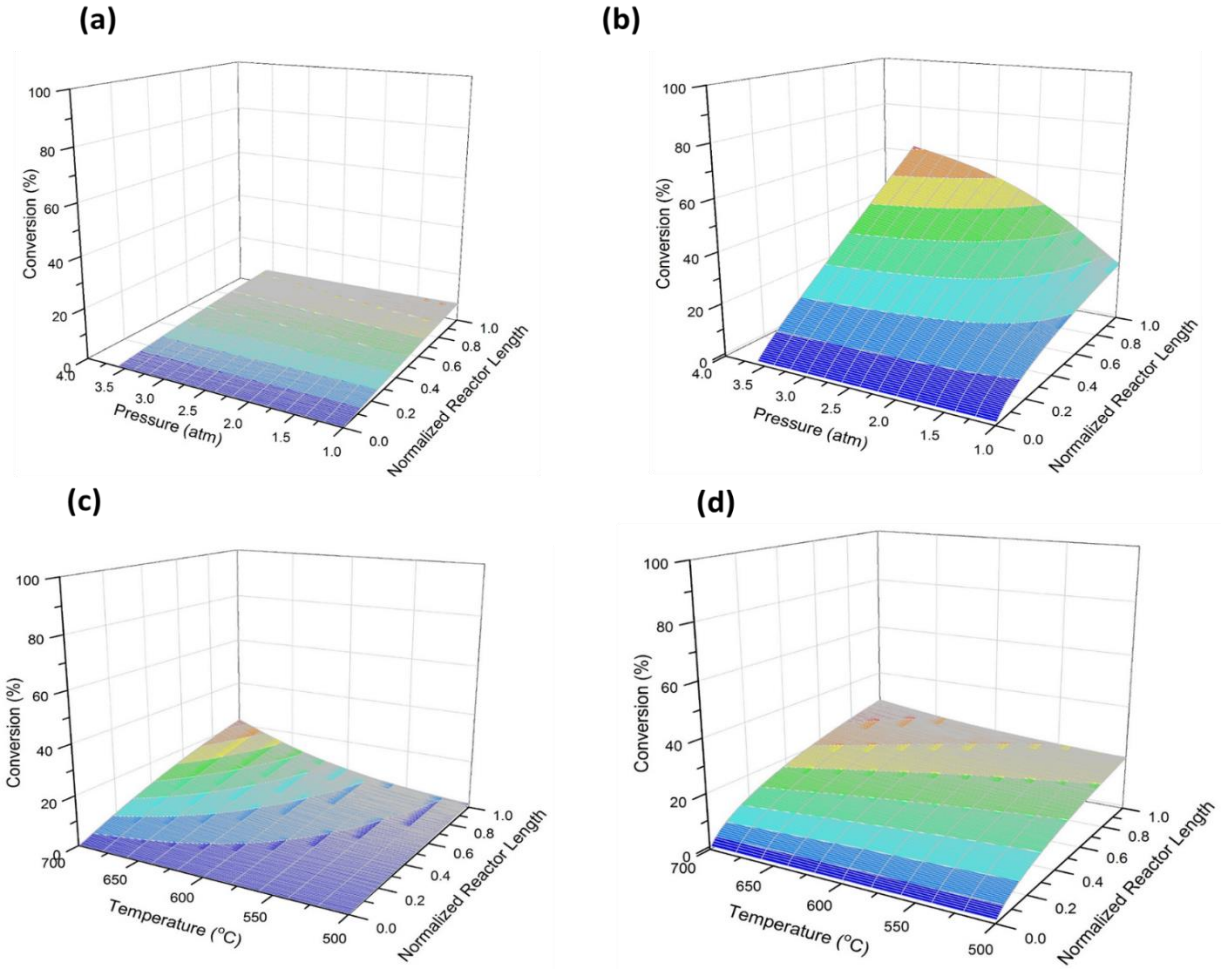

Figure 24. Calculated ethane conversion as a function of pressure along the reactor length in (a) PBR and (b) PBMR at WHSV = 0.45 h^{-1} and temperature= 600 °C and as a function of temperature along the reactor length (c) PBR and (d) PBMR at WHSV = 0.45 h^{-1} and *pfeed*= 1 atm.

Fig. 24 shows the ethane conversion calculated by the 1D PFR model along the reactor length for PBMR and PBR. The maximum ethane conversion observed along the membrane length resulted from the competition between the ethane consumption and gas permeations. For PBR, the ethane conversion gradually increased along the reactor length because of the continuously decreasing ethane partial pressure in the reaction side. In comparison, for PBMR, the rapidness of the increase in ethane conversion in the beginning part of the reactor is strongly due to the H_2 generation and H_2 permeation. The maximum ethane conversion level in PBMR depends upon the reaction temperature and pressure. High temperatures and pressures favor both the ethane consumption (and H_2 generation) and H_2 permeation that lead to greater enhancement of ethane conversion.

5.3. Summary

A model was also developed under the assumption of plug flow conditions and negligible side reaction to not only validate experimental results but also to evaluate ethane conversion beyond experimental conditions. The model developed was verified with comparing its results with the experimental values. The calculated values were in agreement with the experimental results. However, for PBMR the model slightly overestimated the values which can be explained by the decrease in actual permeance values for ethane, ethylene and H_2 in the experiment as the reaction proceeds, which is not taken into account in the model.

In the case of PBR, there are substantial side reactions producing multiple by-products such as methane, propane, and propylene therefore for PBR conversion values from the experiment are higher than those from the model. Moreover, model was used to further investigate the possibility of near complete ethane conversion. Different 3d plots in section 5.2.2 shows the impact of reactor operating conditions on ethane conversion. For a space velocity of 0.45 h^{-1} the highest obtained ethane conversion was 96% at T >750 °C and p_{feed} >3.5 atm. Effect of pressure, temperature and space velocity and F_{Ar} was studied extensively. The impact of H_2 permeance, membrane area and reactor length was also investigated.

Chapter 6

Conclusions

The experimental and simulation studies of this work demonstrated that the porous MFI-type zeolite membranes with moderate H_2 selectivity and H_2 permeance can be useful in ethane dehydrogenation (EDH) reaction using packed bed membrane reactors (PBMR) to effectively enhance the ethane conversion and overcome the equilibrium limit. Use of MFI zeolite membrane helped in exceeding the equilibrium limit of EDH reaction due to the selective permeation of H_2 across the membrane. The ethane conversion, ethylene selectivity, and ethylene yield in the MFI-type zeolite PBMR were higher than in packed bed reactor (PBR). Moreover, the impact of WHSV and sweep gas flow rate (F_{Ar}) were also investigated and found to be critical to the PBMR performance. For the current small-size PBMR, the 1D PFR model was found to work well for simulating the EDH membrane reaction especially for operations under high temperatures and low WHSVs. The modelling results showed a holistic impact of all the operating conditions on performance parameters which could be very helpful in deciding the operating conditions for mass industrial productions. The simulation results suggested that the current zeolite PBMR, although only possessing moderate H_2 selectivity ($\alpha_{H2/C2H6} \sim 3.3$, and $\alpha_{H2/C2H4} \sim 3$) and permeance ($P_{m,H2} < 1.3\times10^{-7}$ mol m^{-2} s^{-1} Pa^{-1}), could achieve ethane conversion of > 98% under practically meaningful operation conditions (e.g., at >600 °C, ~3.5 atm, and F_{Ar} of ~20 cm^3/min). Because of its excellent hydrothermal stability and chemical resistance in a high

EDH reaction environment, the MFI-type zeolite membranes are potentially useful for constructing PBMR for high-temperature EDH reaction.

Bibliography of SHAILESH SINGH DANGWAL

Education

M.S. in Chemical Engineering, (2016-2017), Oklahoma State University, OK

B.-Tech. in Chemical Engineering (2008-2012) Indian Institute of Technology Guwahati, India

Professional Experience

Jan. 2016- Jun. 2017: Research Assistant, Oklahoma State University, OK

Jul. 2012-Dec. 2016: Senior Engineer at Orient Cement Limited, Hyderabad, India

PEER REVIEWED PUBLICATIONS DURING M.S. STUDY

1. Publication: Shailesh Dangwal, Ruochen Liu, S.-J. Kim, High Temperature Ethane Dehydrogenation in Microporous Zeolite Membrane Reactor, Chem. Eng. J. (2017) (under review).

CONFERENCE PRESENTATION

1. Presentation: Shailesh Dangwal, Ruochen Liu, S.-J. Kim, High Temperature Ethane Dehydrogenation in Microporous Zeolite Membrane Reactor, AIChE Annual Meeting, San Francisco, 2016.
2. Presentation: Ruochen Liu, Shailesh Dangwal, S.-J. Kim, MFI-Type Zeolite-Coated Stainless Steel Mesh for Effective Water/Oil Separation, Student Water Conference, Oklahoma State University, Stillwater, 2017.

References

[1] A. Avila, Z. Yu, S. Fazli, J. Sawada, S. Kuznicki, Hydrogen-selective natural mordenite in a membrane reactor for ethane dehydrogenation, Microporous Mesoporous Mater. 190 (2014) 301-308.

[2] Z. Yu, Ethane dehydrogenation using a catalytic membrane reactor, Ph.D. Dissertation, University of Alberta, 2014.

[3] V. Galvita, G. Siddiqi, P. Sun, A.T. Bell, Ethane dehydrogenation on Pt/Mg(Al)O and PtSn/Mg(Al)O catalysts, J. Catal. 271 (2010) 209-219.

[4] O.O. James, S. Mandal, N. Alele, B. Chowdhury, S. Maity, Lower alkanes dehydrogenation: Strategies and reaction routes to corresponding alkenes, Fuel Process. Technol 149 (2016) 239-255.

[5] M.P. Lobera, S. Escolástico, J.M. Serra, High ethylene production through oxidative dehydrogenation of ethane membrane reactors based on fast oxygen-ion conductors, ChemCatChem 3 (2011) 1503-1508.

[6] W.R. True, Global ethylene capacity poised for major expansion, Oil & gas journal 111 (2013) 90-95.

[7] Y. Khojasteh Salkuyeh, New Polygeneration Processes for Power Generation and Liquid Fuel Production with Zero CO2 Emissions, 2015.

[8] F. Ullmann, W. Gerhartz, Y.S. Yamamoto, F.T. Campbell, R. Pfefferkorn, J.F. Rounsaville, Ullmann's encyclopedia of industrial chemistry, Vch Weinheim, Germany1985.

[9] S. Kallus, P. Langlois, G. Romanos, T. Steriotis, E. Kikkinides, N. Kanellopoulos, J. Ramsay, " NCSR DEMOKRITOS, Institute of Physical Chemistry, 15310 Ag, Paraskevi Attikis, Greece, Characterisation of Porous Solids V 128 (2000) 467.

[10] J. Dong, Y. Lin, W. Liu, Multicomponent hydrogen/hydrocarbon separation by MFI-type zeolite membranes, AIChE Journal 46 (2000) 1957-1966.

[11] J.H. Moon, C.H. Lee, Hydrogen separation of methyltriethoxysilane templating silica membrane, AIChE journal 53 (2007) 3125-3136.

[12] K.S. Rothenberger, A.V. Cugini, B.H. Howard, R.P. Killmeyer, M.V. Ciocco, B.D. Morreale, R.M. Enick, F. Bustamante, I.P. Mardilovich, Y.H. Ma, High pressure hydrogen permeance of porous stainless steel coated with a thin palladium film via electroless plating, Journal of membrane science 244 (2004) 55-68.

[13] M.B. Shiflett, H.C. Foley, Ultrasonic deposition of high-selectivity nanoporous carbon membranes, Science 285 (1999) 1902-1905.

[14] Z. Tang, J. Dong, T.M. Nenoff, Internal surface modification of MFI-type zeolite membranes for high selectivity and high flux for hydrogen, Langmuir 25 (2009) 4848-4852.

[15] M. Tsapatsis, G. Xomeritakis, H. Hillhouse, S. Nair, V. Nikolakis, G. Bonilla, Z. Lai, Zeolite membranes, Cattech 3 (1999) 148-163.

[16] Z. Zheng, Synthesis and characterization of ultramicroporous zeolitic membranes for hydrogen separation, University of Cincinnati, 2008.

[17] D. Lewis, C. Freeman, C. Catlow, Predicting the templating ability of organic additives for the synthesis of microporous materials, The Journal of Physical Chemistry 99 (1995) 11194-11202.

[18] J. Dong, Y. Lin, M.Z.-C. Hu, R.A. Peascoe, E.A. Payzant, Template-removal-associated microstructural development of porous-ceramic-supported MFI zeolite membranes, Microporous and mesoporous materials 34 (2000) 241-253.

[19] J. Dong, Y. Lin, M. Kanezashi, Z. Tang, Microporous inorganic membranes for high temperature hydrogen purification, Journal of Applied Physics 104 (2008) 13.

[20] S. Battersby, M.C. Duke, S. Liu, V. Rudolph, J.C.D. da Costa, Metal doped silica membrane reactor: operational effects of reaction and permeation for the water gas shift reaction, Journal of Membrane Science 316 (2008) 46-52.

[21] W. Koros, Y. Ma, T. Shimidzu, Terminology for membranes and membrane processes (IUPAC Recommendations 1996), Pure and Applied Chemistry 68 (1996) 1479-1489.

[22] S.-J. Kim, High Temperature Water Gas Shift Reaction in Zeolite Membrane Reactors, University of Cincinnati, 2011.

[23] J. Caro, M. Noack, Zeolite membranes–recent developments and progress, Microporous and Mesoporous Materials 115 (2008) 215-233.

[24] J. Coronas, J. Santamaria, State-of-the-art in zeolite membrane reactors, Topics in Catalysis 29 (2004) 29-44.

[25] A. Brunetti, A. Caravella, G. Barbieri, E. Drioli, Simulation study of water gas shift reaction in a membrane reactor, Journal of Membrane Science 306 (2007) 329-340.

[26] J. Caro, M. Noack, P. Kölsch, R. Schäfer, Zeolite membranes–state of their development and perspective, Microporous and mesoporous materials 38 (2000) 3-24.

[27] Y. Lin, I. Kumakiri, B. Nair, H. Alsyouri, Microporous inorganic membranes, Separation & Purification Reviews 31 (2002) 229-379.

[28] P. Sun, G. Siddiqi, W.C. Vining, M. Chi, A.T. Bell, Novel Pt/Mg(In)(Al)O catalysts for ethane and propane dehydrogenation, J. Catal. 282 (2011) 165-174.

[29] R. Gudgila, C.A. Leclerc, Support effects on the oxidative dehydrogenation of ethane to ethylene over platinum catalysts, Ind Eng Chem Res 50 (2011) 8438-8443.

[30] J. Wu, Dehydrogenation of light alkanes over supported Pt catalysts, Ph.D. Dissertation, University of California, Berkeley, 2015.

[31] S. Håkonsen, J. Walmsley, A. Holmen, Ethene production by oxidative dehydrogenation of ethane at short contact times over Pt-Sn coated monoliths, Appl. Catal., A 378 (2010) 1-10.

[32] C.A. Gärtner, A.C. van Veen, J.A. Lercher, Oxidative dehydrogenation of ethane: common principles and mechanistic aspects, ChemCatChem 5 (2013) 3196-3217.

[33] E. Gobina, R. Hughes, Ethane dehydrogenation using a high-temperature catalytic membrane reactor, J. Membr. Sci. 90 (1994) 11-19.

[34] E. Gobina, K. Hou, R. Hughes, Ethane dehydrogenation in a catalytic membrane reactor coupled with a reactive sweep gas, Chem. Eng. Sci. 50 (1995) 2311-2319.

[35] E. Gobina, R. Hughes, Reaction assisted hydrogen transport during catalytic dehydrogenation in a membrane reactor, Appl. Catal., A 137 (1996) 119-127.

[36] A. Champagnie, T. Tsotsis, R. Minet, E. Wagner, Ethane dehydrogenation in a catalytic membrane reactor, ChemInform 23 (1992).

[37] J. Szegner, K.L. Yeung, A. Varma, Effect of catalyst distribution in a membrane reactor: experiments and model, AlChE J. 43 (1997) 2059-2072.

[38] D. Ahchieva, M. Peglow, S. Heinrich, L. Mörl, T. Wolff, F. Klose, Oxidative dehydrogenation of ethane in a fluidized bed membrane reactor, Appl. Catal., A 296 (2005) 176-185.

[39] S.-J. Kim, Z. Xu, G.K. Reddy, P. Smirniotis, J. Dong, Effect of pressure on high-temperature water gas shift reaction in microporous zeolite membrane reactor, Ind. Eng. Chem. Res. 51 (2012) 1364-1375.

[40] S.-J. Kim, S. Yang, G.K. Reddy, P. Smirniotis, J. Dong, Zeolite membrane reactor for high-temperature water-gas shift reaction: effects of membrane properties and operating conditions, Energy Fuels 27 (2013) 4471-4480.

[41] Z. Tang, S.-J. Kim, G.K. Reddy, J. Dong, P. Smirniotis, Modified zeolite membrane reactor for high temperature water gas shift reaction, J. Membr. Sci. 354 (2010) 114-122.

[42] S.-J. Kim, S. Tan, M. Taborga Claure, L. Briones Gil, K.L. More, Y. Liu, J.S. Moore, R.S. Dixit, J.G. Pendergast Jr, D.S. Sholl, One-step synthesis of zeolite membranes containing catalytic metal nanoclusters, ACS Appl. Mater. Interfaces 8 (2016) 24671-24681.

[43] S.-J. Kim, Y. Liu, J.S. Moore, R.S. Dixit, J.G. Pendergast Jr, D. Sholl, C.W. Jones, S. Nair, Thin hydrogen-selective SAPO-34 zeolite membranes for enhanced conversion and selectivity in propane dehydrogenation membrane reactors, Chem. Mater. 28 (2016) 4397-4402.

[44] Z. Tang, S.-J. Kim, X. Gu, J. Dong, Microwave synthesis of MFI-type zeolite membranes by seeded secondary growth without the use of organic structure directing agents, Microporous Mesoporous Mater. 118 (2009) 224-231.

[45] J. Szegner, K.L. Yeung, A. Varma, Effect of catalyst distribution in a membrane reactor: experiments and model, AlChE J. 43 (1997) 2059-2072.

[46] E. Gbenedio, Z. Wu, I. Hatim, B.F. Kingsbury, K. Li, A multifunctional Pd/alumina hollow fibre membrane reactor for propane dehydrogenation, Catal. Today 156 (2010) 93-99.

[47] Z. Wu, I. Hatim, B.F. Kingsbury, E. Gbenedio, K. Li, A novel inorganic hollow fiber membrane reactor for catalytic dehydrogenation of propane, AlChE J. 55 (2009) 2389-2398.

[48] E. Simón, J.M. Rosas, A. Santos, A. Romero, Coke formation in copper catalyst during cyclohexanol dehydrogenation: Kinetic deactivation model and catalyst characterization, Chem. Eng. J. 214 (2013) 119-128.

[49] P.L. Benito, A.G. Gayubo, A.T. Aguayo, M. Castilla, J. Bilbao, Concentration-dependent kinetic model for catalyst deactivation in the MTG process, Ind. Eng. Chem. Res. 35 (1996) 81-89.

[50] A.C. Bose, Inorganic membranes for energy and environmental applications, Springer 2009, p. 307-308.

[51] M. Hasany, M. Malakootikhah, V. Rahmanian, S. Yaghmaei, Effect of hydrogen combustion reaction on the dehydrogenation of ethane in a fixed-bed catalytic membrane reactor, Chin. J. Chem. Eng. 23 (2015) 1316-1325.

[52] M.L. Rodriguez, D.E. Ardissone, E. Heracleous, A.A. Lemonidou, E. López, M.N. Pedernera, D.O. Borio, Oxidative dehydrogenation of ethane to ethylene in a membrane reactor: A theoretical study, Catal. Today 157 (2010) 303-309.

[53] N. Hansen, R. Krishna, J. van Baten, A. Bell, F. Keil, Reactor simulation of benzene ethylation and ethane dehydrogenation catalyzed by ZSM-5: A multiscale approach, Chem. Eng. Sci. 65 (2010) 2472-2480.

Appendix

The code for the EDH PBMR is as follows

```
% EDH Reaction

% Membrane Parameters

Mc=0.55;              % Mass of catalyst in g

A=1.34E-06;           % Area of membrane in m^2

A1=3.14*A;

S= 0.45;              % Space velocity in h^-1

K0=4.17468541820873E-4; % Constant in rate constant equation mol/s.m^2.pascal

E0= 86192.46862;          % Activation energy in J/mol

MEt=40;               % Molecular weight of ethane in g

Mh2=2;                % Molecular weight of hydrogen in g

MEty=28;              % Molecular weight of ethylene in g

VEt=1.5;              % Flow rate of ethane in ccm

VEty=0;               % Flow rate of ethylene in ccm

Vh2=0;                % Flow rate of hydrogen in ccm

VAr=20;               % Flow rate of argon in ccm

s=1;                  %Pressure of feed side in atm

P_r=101325*s;         % Pressure in retentate side in pascal

P_p=101325;           % Pressure in permeate side in pascal

R=8.314;              % Universal gas constant J/mol-K
```

```
%DEt=4.08E-4;          % Density of ethane in mol/cc
%DEty=4.08E-4;         % Density of ethylene in mol/cc
%Dh2= 4.08E-4;         % Density of hydrogen in mol/cc
%DAr=4.08E-4;          % Density of argon in mol/cc
%DEt=0.0000453;        % Density of ethane in mol/cc
%DEty=0.00004214;      % Density of ethylene in mol/cc
%Dh2= 0.00004494;      % Density of hydrogen in mol/cc
%DAr=0.0000446;        % Density of argon in mol/cc
% Mole Fractions in Feed
yEt=1;                 % Mole fraction for ethane in feed
yEty=0.0000001;        % Mole fraction for ethylene in feed
yh2=0.0000001;         % Mole fraction for hydrogen in feed
yAr=0;                 % Mole fraction for argon in feed

% Mole Fractions in permeate side
yEtp=0;                % Mole fraction for ethane in permeate
yEtyp=0;               % Mole fraction for ethylene in permeate
yh2p=0;                % Mole fraction for hydrogen in permeate
yArp=1;                % Mole fraction for argon in permeate
T=873;                 % Temperature in kelvin
% Molar flow rates of components in feed
FEt=(VEt*P_r*0.000001)/(R*T*60);      % Molar flow rate of ethane in mol/min
FEti=FEt;                             % Storing initial value for final conversion calculation
```

```
FEty=(VEty*P_r*0.000001)/(R*T*60);      % Molar flow rate of ethylene in mol/min
Fh2=(Vh2*P_r*0.000001)/(R*T*60);        % Molar flow rate of hydrogen in mol/min
FAr=0;
% Partial pressures of components in feed
PEt=P_r*yEt;         % Partial pressure for ethane in pascal
PEty=P_r*yEty;       % Partial pressure for ethylene in pascal
Ph2=yh2*P_r;         % Partial pressure for hydrogen in pascal
PAr=yAr*P_r;
% Molar flow rates of components in sweep gas
FArp=(VAr*P_r*0.000001)/(R*T*60);
FEtp=0;          % Molar flow rate of ethane in mol/min in permeate
FEtyp=0;         % Molar flow rate of ethylene in mol/min in permeate
Fh2p=0;          % Molar flow rate of hydrogen in mol/min in permeate
%Equilibrium constant
keq=101325*7280000*exp((-17000)/T);          % Equilibrium constant in pascal
k=K0*exp((-E0)/(T*R));                       % rate constant in mol/s.m2.pascal

    % Calculaton of permeance
     Pmh2=6.2E-08;                    % Permeance of hydrogen (mol/s.m2.pascal)
     PmEty=1.62E-08;          % Permeance of ethylene (mol/s.m2.pascal)
     PmEt=1.3E-08;                    % Permeance of ethane (mol/s.m2.pascal)
     PmAr=9.44E-08;                   % Permeance of argon (mol/s.m2.pascal)
     %PmEt=0.0000000198*exp(0.0002*(T-273));          % Permeance of ethane (mol/s.m2.pascal)
```

```
%PmEty=0.0000000259*exp(0.0001*(T-273));          % Permeance of ethylene (mol/s.m2.pascal)
%Pmh2=0.0000000245*exp(0.0034*(T-273));           % Permeance of hydrogen (mol/s.m2.pascal)
Results=zeros(150,3);
for i=1:150                                       % No of sections
i;
Rate=k*(PEt-((PEty*Ph2)/(keq)));                  % Mol/s.m2
% Differential pressure for each component across membrane
dpEt=P_r*yEt-P_p*yEtp;                % Differential pressure for ethane in pascal
dpEty=P_r*yEty-P_p*yEtyp;             % Differential pressure for ethylene in pascal
dph2=P_r*yh2-P_p*yh2p;                % Differential pressure for hydrogen in pascal
dpAr=P_r*yAr-P_p*yArp;                % Differential pressure for argon in pascal
% Molar flow rate of each component in permeate
%FEtp=FEtp+PmEt*A*dpEt*60;            % Molar flow rate of ethane in mol/min in permeate
%FEtyp=FEtyp+PmEty*A*dpEty*60;        % Molar flow rate of ethylene in mol/min in permeate
%Fh2p=Fh2p+Pmh2*A*dph2*60;            % Molar flow rate of hydrogen in mol/min in permeate
%Ftp=FEtyp+Fh2p+FAr;                  % Total molar flow rate in permeate in mol/min
FEtp=FEtp+PmEt*A*dpEt;                % Molar flow rate of ethane in mol/min in permeate
FEtyp=FEtyp+PmEty*A*dpEty;            % Molar flow rate of ethylene in mol/min in permeate
Fh2p=Fh2p+Pmh2*A*dph2;                % Molar flow rate of hydrogen in mol/min in permeate
FArp=FArp+PmAr*A*dpAr;                % Molar flow rate of argon in mol/min in permeate
Ftp=FEtp+FEtyp+Fh2p+FArp;             % Total molar flow rate in permeate in mol/min

% Calculation of flux through the membranes
```

```
FluxEtp=FEtp/(A);                % Flux of ethane across the membrane in mol/s.m2
FluxEtyp=FEtyp/(A);              % Flux of ethylene across the membrane in mol/s.m2
Fluxh2p=Fh2p/(A);                % Flux of hydrogen across the membrane in mol/s.m2

% Molar flow rate of each component in retentate
FEt=FEt-Rate*A-PmEt*A1*dpEt;     % Molar flow rate of ethane in mol/min
FEty=FEty+Rate*A-PmEty*2*A1*dpEty;  % Molar flow rate of ethylene in mol/min
Fh2=Fh2+Rate*A-Pmh2*A1*2*dph2;   % Molar flow rate of hydrogen in mol/min
FAr=FAr+Rate*A-PmAr*2*A1*dpAr;   % Molar flow rate of argon in mol/min
Ft=FEt+FEty+Fh2+FAr;             % Total molar flow rate in retentate in mol/min

Results(i,1) = yEt;              % Saving ethane mole fraction
Results(i,2) = yEty;             % Saving ethylene mole fraction
Results(i,3) = yh2;              % Saving hydrogen mole fraction

% Mole fraction of each component in permeate
yEtp=FEtp/Ftp;                   % Mole fraction of ethane in permeate
yEtyp=FEtyp/Ftp;                 % Mole fraction of ethylene in permeate
yh2p=Fh2p/Ftp;                   % Mole fraction of eydrogen in permeate
yArp= FArp/Ftp;                  % Mole fraction of argon in permeate

% Mole fraction of each component in retentate
yEt=FEt/Ft;                      % Mole Fraction for ethane in retentate
```

```
  yEty=FEty/Ft;              % Mole fraction for ehylene in retentate
  yh2=Fh2/Ft;                % Mole fraction for hydrogen in retentate
  yAr=FAr/Ft;                % Mole fraction for argon in retentate

  % Caluculation of revised partial pressures in retentate side
  PEt=P_r*yEt;               % Revised partial pressure of ethane in retentate in pascal
  PEty=P_r*yEty;             % Revised partial pressure of ethylene in retentate in pascal
  Ph2=P_r*yh2;               % Revised partial pressure of argon in retentate in pascal
  X=(FEti-FEt-FEtp)/(FEti);  % Conversion after section i

  Results(i,4) = X;          % Storing conversion after section i
end

FEt                          % Printing ethane exit flow rate from retentate in mol/min
FEtp                         % Printing ethylene exit flow rate from retentate in mol/min
FEti                         % Printing ethane inlet flow rate in mol/min
X=(FEti-FEt-FEtp)/(FEti)     % Printing overall ethane conversion
```

VITA

Shailesh Singh Dangwal

Candidate for the Degree of

Master of Science

Thesis: HIGH-TEMPERATURE ETHANE DEHYDROGENATION IN MICROPOROUS ZEOLITE MEMBRANE REACTOR: EFFECT OF OPERATING CONDITIONS

Major Field: Chemical Engineering

Biographical:

Shailesh Singh Dangwal was born in Ghaziabad, India and grew up in Ghaziabad, India.

Education:

Completed the requirements for the Master of Science in Chemical Engineering at Oklahoma State University, Stillwater, Oklahoma in June, 2017.

Completed the requirements for the Bachelor of Science in Chemical Engineering at Indian Institute of Technology, Guwahati, India in 2012.

Experience:

Worked as Graduate Research Assistant in the department of Chemical Engineering at Oklahoma State University, Stillwater from August 2014 to July 2016

Also worked as senior Engineer in Orient Cement Limited from July 2012 to December 2016 at Hyderabad, India

Professional Memberships:

Student member of CHEGSA